A Numerical Study on the Influences of Sumatra Topography and Synoptic Features on Tropical Cyclone Formation over the Indian Ocean

CHUNG-CHIEH WANG AND SHIN-KAI MA

Department of Earth Sciences, National Taiwan Normal University, Taipei, Taiwan

RICHARD H. JOHNSON

Department of Atmospheric Sciences, Colorado State University, Fort Collins, Colorado

(Manuscript received 6 August 2019, in final form 23 April 2020)

ABSTRACT

Spanning across the equator with a northwest–southeast orientation, the island of Sumatra can exert significant influences on low-level flow. Under northeasterly flow, in particular, lee vortices can form and some of them may subsequently develop into tropical cyclones (TCs) in the Indian Ocean (IO). Building upon the recent work of Fine et al., this study investigates the roles of the Sumatra topography and other common features on the formation of selected cases for analysis and numerical experiments. Four cases in northern IO were selected for analysis and two of them [Nisha (2008) and Ward 2009)] for simulation at a grid size of 4 km. Sensitivity tests without the Sumatra topography were also performed. Our results indicate that during the lee stage, most pre-TC vortices tend to be stronger with a clearer circulation when the topography is present. However, the island's terrain is a helpful but not a deciding factor in TC formation. Specifically, the vortices in the no-terrain tests also reach TC status, but just at a later time. Some common ingredients contributing to a favorable environment for TC genesis are identified. They include northeasterly winds near northern Sumatra, westerly wind bursts along the equator, and migratory disturbances (TC remnants or Borneo vortices) to provide additional vorticity/moisture from the South China Sea. These factors also appear in most of the 22 vortices in northern IO during October–December in 2008 and 2009. For the sole case (Cleo) examined in southern IO, the deflection of equatorial westerlies into northwesterlies by Sumatra (on the windward side) is also helpful to TC formation.

1. Introduction

The formation of a tropical cyclone (TC) is regarded as a complex process that involves continuous and nonlinear interaction among mechanisms across a wide range of scales, rather than controlled by a single mechanism. Since Ooyama (1982), tropical cyclogenesis is considered the transition from the probabilistic to deterministic stage in the life cycle of a TC. In the probabilistic stage with weak relative vorticity ζ (and absolute vorticity η), tropical cloud clusters typically have large Rossby radius of deformation (λ_R) and low heating efficiency from latent heat release, and most of them have short life spans and do not intensify into TCs.

Past studies have established the synoptic conditions conducive to TC formation (e.g., Gray 1968): deep ocean mixing layer with sea surface temperature (SST) at least 26.5°C, unstable atmospheric environment, high moisture content in low and middle levels, weak vertical wind shear, a latitude outside 5° (nonzero Coriolis force), and high low-level vorticity. However, even when all the above conditions are met in the probabilistic stage, it only means a higher likelihood for TC genesis. The cloud cluster (and initial vortex) still needs external forcing mechanism(s) to increase its vorticity, reduce the λ_R, and subsequently raise the heating efficiency of latent heat released in cumulus convection. Only after that, the disturbance can survive the probabilistic stage and enter the deterministic stage with positive feedback in development through the mechanisms of angular momentum conservation and conditional instability of the second kind (CISK; Charney and Eliassen 1964) or wind-induced surface heat exchange (WISHE; Emanuel 1986; Rotunno and Emanuel 1987).

Corresponding author: Prof. Chung-Chieh Wang, cwang@ntnu.edu.tw

DOI: 10.1175/MWR-D-19-0259.1

For individual disturbances, some external forcing mechanism, or mechanisms, is an essential element for TC formation, besides favorable environmental conditions. In the western North Pacific (WNP), for example, Ritchie and Holland (1999) identified five large-scale circulation features or processes that can force or are linked to TC formation: monsoon shear lines, monsoon gyres, easterly waves, monsoon confluence regions, and Rossby energy dispersion. The observational study of Lee (1986) also points out the importance of low-level momentum forcing in TC-genesis cases in the WNP. Such momentum forcing over a large area may come from cross-equatorial flow, trade wind surges, or bursts of the Indian monsoon. Through inward transfer of eddy vorticity flux, the forcing can increase the low-level ζ of the TC vortex without a strengthening in its transverse circulation, and act to help the TC to enter the deterministic stage (Lee 1986).

Midlatitude cold-air outbreaks in the opposing hemisphere are usually the source of the cross-equatorial flow (Love 1985a,b), while those in the same hemisphere can initiate trade wind surges. In northern Indian Ocean (NIO) where TCs occur more often during premonsoon and postmonsoon seasons (e.g., Subbaramayya and Rao 1984; Kikuchi and Wang 2010), similar low-level momentum forcings from wind bursts also often promote TC formation there (Lee et al. 1989). In these situations, initially asymmetric shearing vorticity gradually turns into symmetric curvature vorticity as the vortex strengthens. In addition, when a TC forms and intensifies in the IO, its outer circulation can enhance the shearing vorticity in the other hemisphere and this process may lead to TC formation there, resulting in a TC pair across the equator (Lee et al. 1989).

The cold surge helps TC formation not only in WNP and NIO, but also in the South China Sea (SCS; Chang et al. 2005; Lin and Lee 2011). In the winter, when the northeasterly wind surge reaches the SCS, it may provide positive vorticity and lead to the formation of the Borneo vortex (BV). Some semistationary and others westward-moving, these BVs may continue to develop and eventually become a TC if the environment is favorable (Lin and Lee 2011). One such example is Typhoon Vamei (2001) that formed near Singapore very close to the equator (Chang et al. 2003). Through composite analysis, Takahashi et al. (2011) also found that regions of positive vorticity often exist in the SCS and NIO due to strong northeasterly flow during the winter months (October–March), thus contributing to TC formation in these ocean basins.

In addition to the large-scale momentum forcing mentioned above, certain topographic features in the tropics, when encountered by airflow, can act to produce localized vorticity, and therefore play a role in TC formation. One such feature is Central America (the Sierra Madre range in particular), which is argued to affect the formation of hurricanes downstream from the topography in eastern North Pacific (Mozer and Zehnder 1996; Farfán and Zehnder 1997; Zehnder et al. 1999). Results from numerical experiments indicate that lee vortices (Smolarkiewicz and Rotunno 1989; Rotunno and Smolarkiewicz 1991; Epifanio 2003), with a depth of about 3 km, often form downstream of Central America in a low-Froude number (Fr) regime under easterly prevailing wind. The definition of Fr, which gives the overall response of the flow when encountering an obstacle, is $\mathrm{Fr} = U/Nh$, where U is the wind speed perpendicular to the topography, N is buoyancy oscillation frequency, and h is the terrain height. For Central America, both a strong jet through the Tehuantepec gap and flow around topography can produce vorticity to form lee vortices under such conditions. With moisture advection from the intertropical convergence zone (ITCZ), the environment downstream from Central America may become even more favorable to TC development (Zehnder et al. 1999). The above case studies indicate the topography can produce the initial vortex, which can develop into a TC given a suitable environment.

Compared to Central America, the topography of Sumatra at the western end of Maritime Continent is much less studied. Kuettner (1967, 1989) suggests that the unique configuration of Sumatra, which straddles the equator in a way that is found nowhere else in the world, may be an important source for TC pairs in the IO. With a northwest–southeast orientation, the topography of Sumatra extends more than 1600 km (from about 6°N to 6°S) and peaks at about 3.8 km (cf. Fig. 1a). When the winter northeasterly flow reaches Sumatra, lee vortices may form at both ends. While counterrotating, both are cyclonic and may serve as initial vortices and, after shedding, intensify into TCs under a favorable environment (Fig. 1a).

Recently, Fine et al. (2016) examined TCs in the IO using datasets from European Centre for Medium-Range Weather Forecasts (ECMWF) Year of Tropical Convection (YOTC, 2008–10; Waliser et al. 2012) and Dynamics of the Madden–Julian Oscillation (DYNAMO, 2011–12; Johnson and Ciesielski 2013). They found that 31.3% of all TCs in the 2.5-yr study period in NIO can be traced back to the Sumatra area, while the corresponding number for the southern IO (SIO) is 22.9%. These high percentages imply that the topography of Sumatra could play a significant role in providing initial vortices of TCs in IO. For northern (southern) Sumatra, the terrain-induced

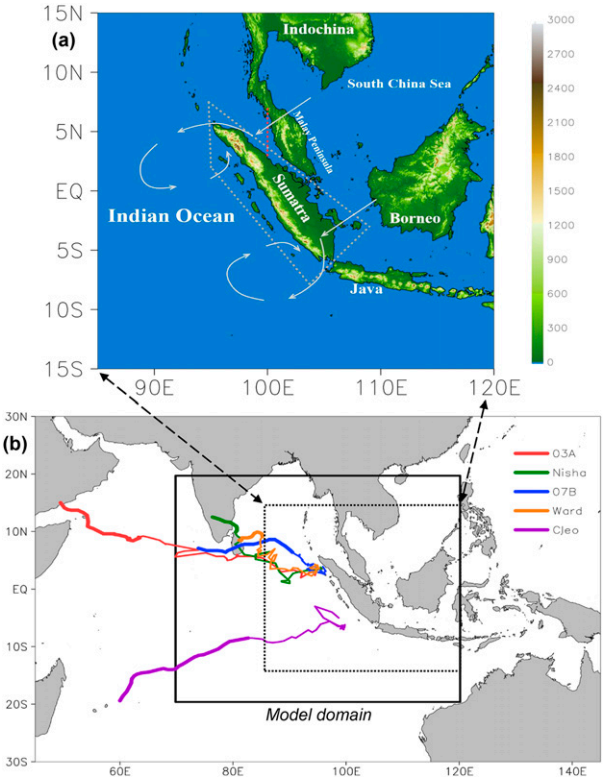

FIG. 1. (a) The topography of Sumatra and surrounding region (m, color), and a schematic of lee vortices based on Kuettner (1967). The gray-dotted polygon shows the area to remove terrain in sensitivity tests, and the red-dotted line shows the segment used to compute Fr. (b) Tracks of the five selected cases (thickened for lifespan reaching TS intensity) and the model simulation domain (thick solid box).

cyclonic vortices are more common during boreal winter (summer) with low-level easterly flow, while TC genesis from them in NIO appear to occur in October–December (Fine et al. 2016), presumably linked to other environmental factors.

Following Fine et al. (2016), which is a preliminary observational and climatological study without an examination on the TC genesis of individual cases, a numerical study seems logical. Therefore, the present study selects a few lee vortex cases during the YOTC period for analysis and numerical simulation. Sensitivity experiments in which the Sumatra topography is removed are also performed, with a goal of clarifying the importance of the topography relative to other potentially helpful factors for TC formation in these cases. These other factors include synoptic ingredients surrounding the lee area as well as vorticity and moisture advection associated with incipient disturbances, such as a BV, from the SCS upstream. This study represents the first numerical investigation of the processes involved in TC formation associated with Sumatra wake vortices as well as the relative importance of other synoptic features in the environment.

2. Data and design of numerical experiments

a. Data and analysis methods

In this study, all the TCs in the NIO during October–December within the YOTC period (May 2008–April 2010, Waliser et al. 2012; Moncrieff et al. 2012) are briefly analyzed (sections 3 and 6), and their basic track and intensity information was taken from the Joint Typhoon Warning Center (JTWC) best track data. The gridded ECMWF-YOTC global analyses (e.g., Moncrieff et al. 2012), available on a 0.25° × 0.25° (latitude–longitude) grid at 20 levels (1000 to 10 hPa) every 6 h, are used for the examination of the synoptic environment and evolution of these storms.

From the 13 cases included in Fine et al. (2016), five TCs that could be linked to Sumatra (during October–December) were selected for a more detailed analysis of the processes of lee vortex formation and the subsequent TC genesis using the ECMWF-YOTC data in section 3. The three stronger TCs, including Nisha (2008) and Ward (2009) in the NIO and Cleo (2009) in the SIO, that became named storms are further chosen for numerical simulation and sensitivity tests. The ECMWF-YOTC data serve as initial and boundary conditions (IC/BCs) for these experiments. Satellite brightness temperature (T_B) imageries provided by the Naval Research Laboratory (NRL) and microwave products from the Space Science and Engineering Center (SSEC, at University of Wisconsin) are also used to help verify model simulations.

In this study, the intensity of tropical storm (TS) of 34 kt (1 kt ≈ 0.51 m s^{-1}) is adopted to identify TC formation in both the observation and model in a consistent way, as the storms are given a name and typically enter the deterministic stage near this time (Ooyama 1982). To analyze their vertical structure and evolution, the centers of the vortices at (or near) 850 hPa are identified and used to compute the mean relative vorticity within 550 km, a radius determined after extensive testing, including the earlier, lee stage of the vortices. To further diagnose the differences between the control experiment and sensitivity test (without the Sumatra terrain) of each TC case, the vorticity equation was employed, and a lag correlation analysis between the vorticity of the lee vortex and the upstream Fr was also carried out to elucidate the topographic effects of the Sumatra Island. Further details of these analyses will be described in sections 4 and 5.

b. Numerical model and experiments

The Cloud-Resolving Storm Simulator (CReSS) version 3.4.2 (Tsuboki and Sakakibara 2002, 2007) is used in

TABLE 1. The CReSS model domain configuration (top), initial and boundary conditions (IC/BCs, middle), and physical schemes (bottom) used in this study.

Cases	Nisha (2008)	Ward and Cleo (2009)
Projection	Mercator, center at 100°E	
Grid spacing (km × km × km)	4.0 × 4.0 × 0.1–0.727 (0.5)[a]	
Grid dimension (x, y, z) and domain size (km × km × km)	1400 × 1116 × 40 (5600 × 4464 × 20)	
IC/BCs (including SST)	ECMWF-YOTC analyses (0.25°, 20 levels, every 6 h)	
Topography	Digital elevation model at (1/120)°	
Initial time	1200 UTC 14 Nov 2008	0000 UTC 29 Nov 2009
Integration length	15 days	16 days
Output frequency	1 h	
Cloud microphysics	Bulk cold rain (Lin et al. 1983; Cotton et al. 1986; Murakami 1990; Ikawa and Saito 1991; Murakami et al. 1994)	
PBL/turbulence	1.5-order closure with prediction of turbulent kinetic energy (Deardorff 1980; Tsuboki and Sakakibara 2007)	
Surface processes	Energy/momentum fluxes, shortwave and longwave radiation (Kondo 1976; Louis et al. 1982; Segami et al. 1989)	
Substrate model	43 levels, every 5 cm to 2.1 m	

[a] The vertical grid spacing (Δz) of CReSS is stretched (smallest at the bottom), and the averaged spacing is given in the parentheses.

this study for all experiments. It is a single-domain, nonhydrostatic and compressible cloud-resolving model with a terrain-following vertical coordinate. In CReSS, clouds are explicitly treated using a bulk cold-rain microphysics scheme with a total of six species (vapor, cloud water, cloud ice, rain, snow, and graupel) without the use of any cumulus parameterization, while subgrid-scale processes such as turbulent mixing in the boundary layer and surface radiation and momentum/energy fluxes are parameterized (Table 1). The CReSS model has been employed in many earlier studies on TCs (Wang 2015; Wang et al. 2012, 2013, 2015, 2016; Chen et al. 2017; Kuo et al. 2019), and the readers are referred to the references therein and Tsuboki and Sakakibara (2002, 2007) for further details.

Two control (CTL) experiments were performed using a large domain of 5600 km × 4464 km (roughly 20°S–20°N, 70°–120°E, Fig. 1b) at a convective-permitting grid size of 4 km, one for Nisha (2008) and the other for Ward (2009) and Cleo (2009) together, since they were twin cyclones across the equator during the same period. Using the YOTC analyses as IC/BCs, these runs started from 6 h before the arrival of low-level northeasterly flow to Sumatra, at 1200 UTC 14 November 2008 for Nisha and 0000 UTC 29 November 2009 for Ward and Cleo, and lasted for 15 and 16 days, respectively (Table 1). For the no-terrain (NT) tests, all model setups and IC/BCs are identical to the CTL, except that the topography of Sumatra (and the small islands nearby) are removed (but the landmass remains, cf. Fig. 1a). Here, it should be noted that the SIO case of Cleo was not a lee vortex, since the northeasterly flow did not extend south of the equator. In fact, none of the SIO TCs examined by Fine et al. (2016) developed from a lee vortex, but as the only SIO case, it is still worthwhile to include Cleo in the present study.

c. *Vorticity budget analysis for lee vortices*

Except for the methods mentioned above in section 2a, the vorticity budget analysis was also performed for the vortices during the lee stage in both CTL and NT experiments for each of the selected cases to further shed lights on their development. The vorticity (tendency) equation in Cartesian and z coordinate can be written as

$$\frac{\partial \zeta}{\partial t} = -\boldsymbol{v}\cdot\nabla\eta - w\frac{\partial \zeta}{\partial z} - \eta(\nabla\cdot\boldsymbol{v}) + \left(\frac{\partial u}{\partial z}\frac{\partial w}{\partial y} - \frac{\partial v}{\partial z}\frac{\partial w}{\partial x}\right) + \frac{1}{\rho^2}\left(\frac{\partial \rho}{\partial x}\frac{\partial p}{\partial y} - \frac{\partial \rho}{\partial y}\frac{\partial p}{\partial x}\right) + \left(\frac{\partial F_y}{\partial x} - \frac{\partial F_x}{\partial y}\right), \quad (1)$$

where the forcing terms on the rhs, following the order, are horizontal advection of η ($= \zeta + f$), vertical advection of ζ, convergence (or vertical stretching) effect, tilting effect, solenoidal effect, and the frictional effect that also accounts for the residual from computational errors. Using Eq. (1), the model results of lee vortices in CTL and NT experiments are compared (sections 4 and 5).

3. Case analysis

The five TCs linked to Sumatra during the data period were selected for analysis in this section, and they are TC 03A (2008), TS Nisha (2008), TC 07B (2008), TS Ward (2009), and TC Cleo (2009), respectively, in chronological order. The first four were in the NIO and developed

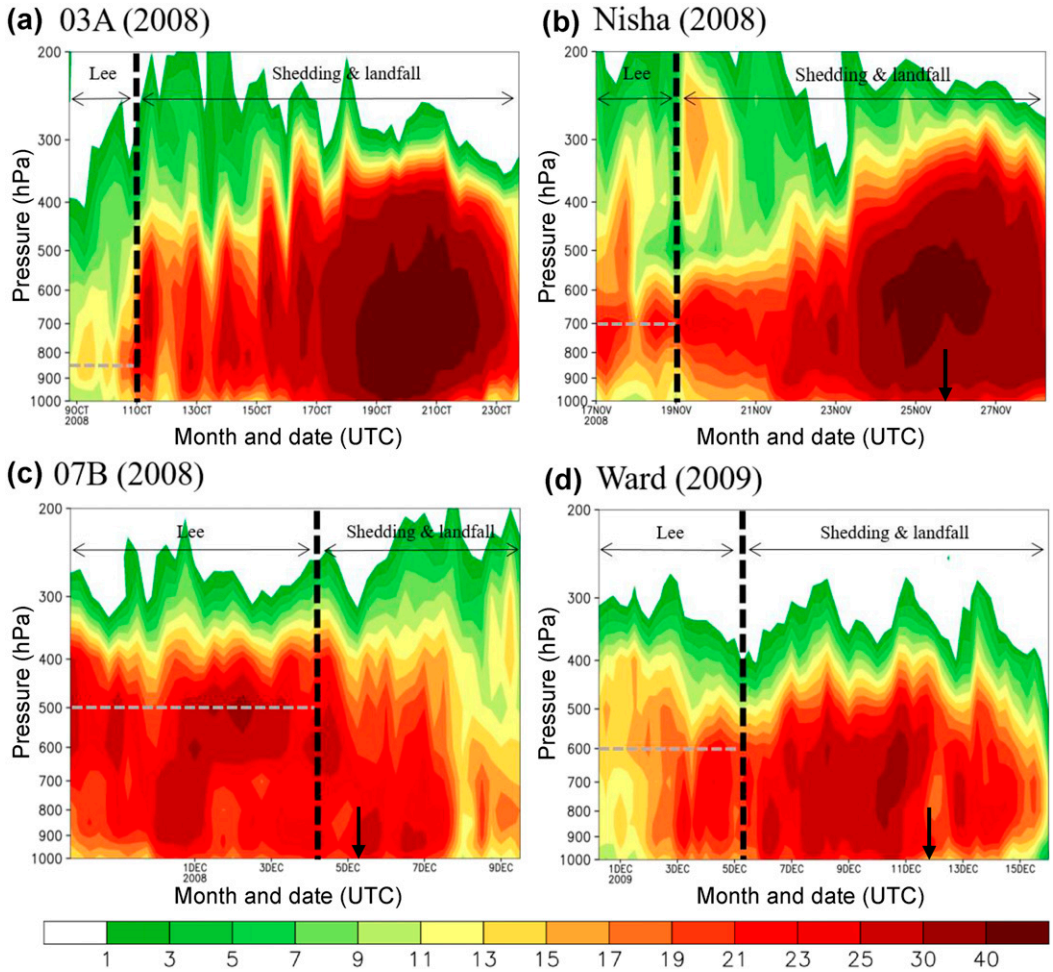

FIG. 2. Time–height section of mean relative vorticity (ζ, $10^{-6}\,s^{-1}$), computed from ECMWF-YOTC data and averaged inside 550 km from the vortex center, for the four cases in NIO: (a) 03A, (b) Nisha, (c) 07B, and (d) Ward. Each panel starts at the time of lee vortex formation. The thick dashed vertical lines mark the time when the vortex started to move downstream, and the arrows denote when the TS intensity is reached in JTWC best track data (not applicable for 03A). The gray dashed horizontal lines depict the level of maximum vorticity.

into TCs from lee vortices of northern Sumatra, while Cleo was in the SIO and formed a TC pair with Ward as mentioned. The full tracks of these five cases, constructed using both YOTC analysis (vortex center at 850 hPa during pre-TS stage) and JTWC best track data (TS and beyond), are shown in Fig. 1b.

Following the methodology described in section 2a, time–height sections of mean relative vorticity ζ inside a radius of 550 km for the four cases in NIO were constructed (Fig. 2). This allowed us to identify the level of maximum (areal-mean) ζ during the leeside stage of the vortices, and these levels were used to show (in Fig. 3) the evolution in wind and vorticity before, during, and after the formation of leeside vortex (t_0), which is taken to be the time when a closed circulation at 850 hPa formed in the ECMWF-YOTC analysis. During the 4-day period, easterly flow appeared near northern Sumatra and to its north in all four cases and generally strengthened during the period (Fig. 3). At the same time, westerly winds intensified at lower latitudes near the equator prior to t_0, except for 03A in which westerlies occurred shortly after t_0 (Fig. 3a). Appearing also in the composite fields of Fine et al. (2016, their Figs. 2a and 6), these two branches of airflow provided cyclonic vorticity and a background environment favorable for lee vortex formation and its subsequent development.

In addition to the opposing flow in the leeside region, clear incipient positive vorticity also existed in Fig. 3 near 110°E at 0°–5°N in the SCS two days before lee vortex formation in all three latter cases, while the one in 03A was weaker and less evident (Fig. 3a). Note that 03A is the only case among the four that did not reach

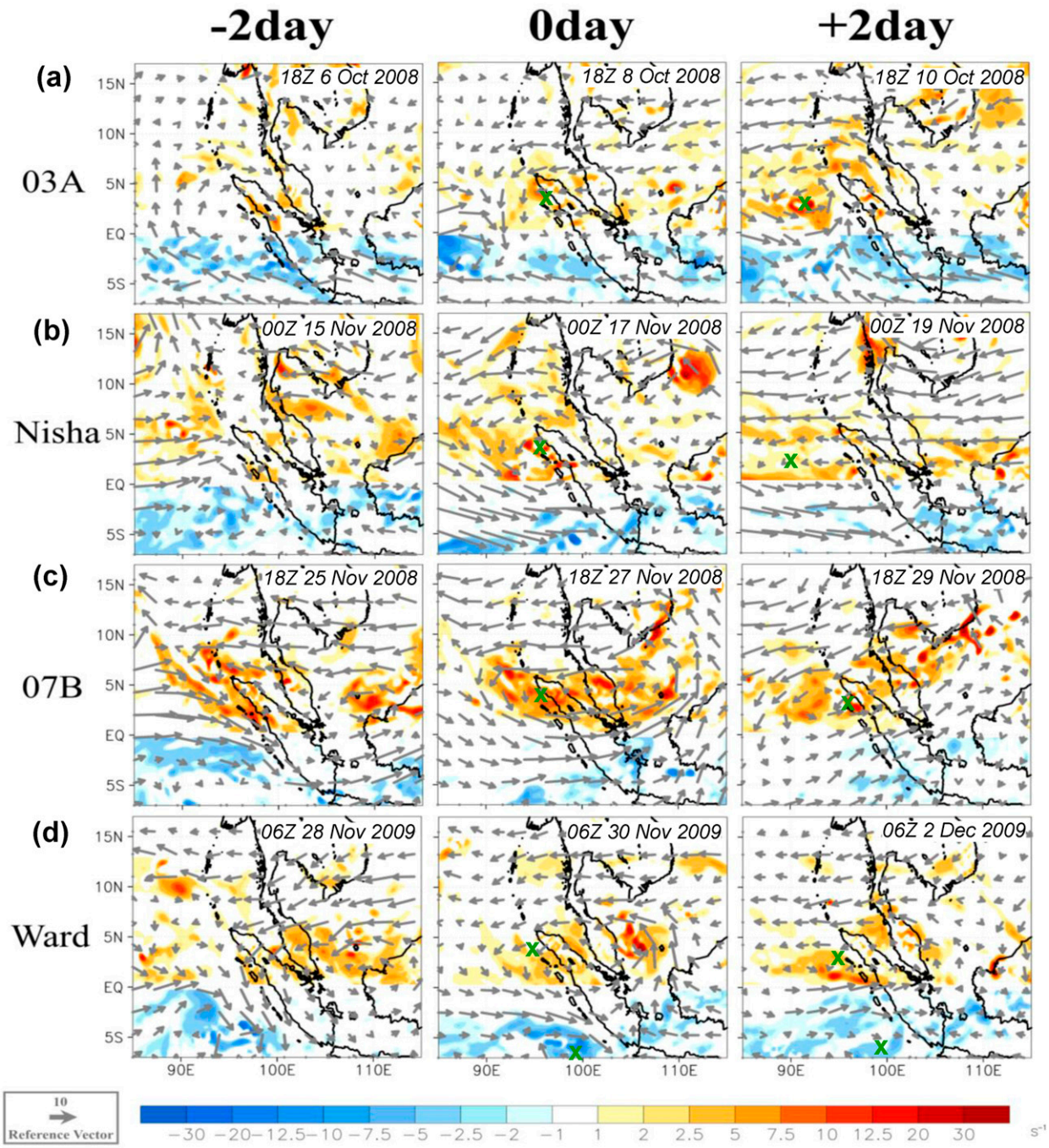

FIG. 3. Distributions of horizontal wind (gray vectors, m s^{-1}) and relative vorticity (10^{-5} s^{-1}, color, cyclonic only) in ECMWF-YOTC data (left) two days before, (middle) at the time of, and (right) two days after the formation of the lee vortex for (a) 03A at 850 hPa, (b) Nisha at 700 hPa, (c) 07B at 500 hPa, and (d) Ward at 600 hPa. Both the reference vector and color scales are plotted at the bottom. The vortex centers at 850 hPa are marked by a green "×" [not necessarily the same as the center at the level shown in (b)–(d)].

TS status (cf. Fig. 2a). These vorticity centers were either from the remnants of tropical systems or associated with a BV and moved westward to reach the lee side of northern Sumatra at t_0, when the lee vortex subsequently formed. Afterward, the lee vortex in all four cases gradually shed and moved downstream, away from Sumatra (Figs. 1a, 3). In longitude–time (Hovmöller) plots (Fig. 4), the incipient disturbances can be identified to be from the

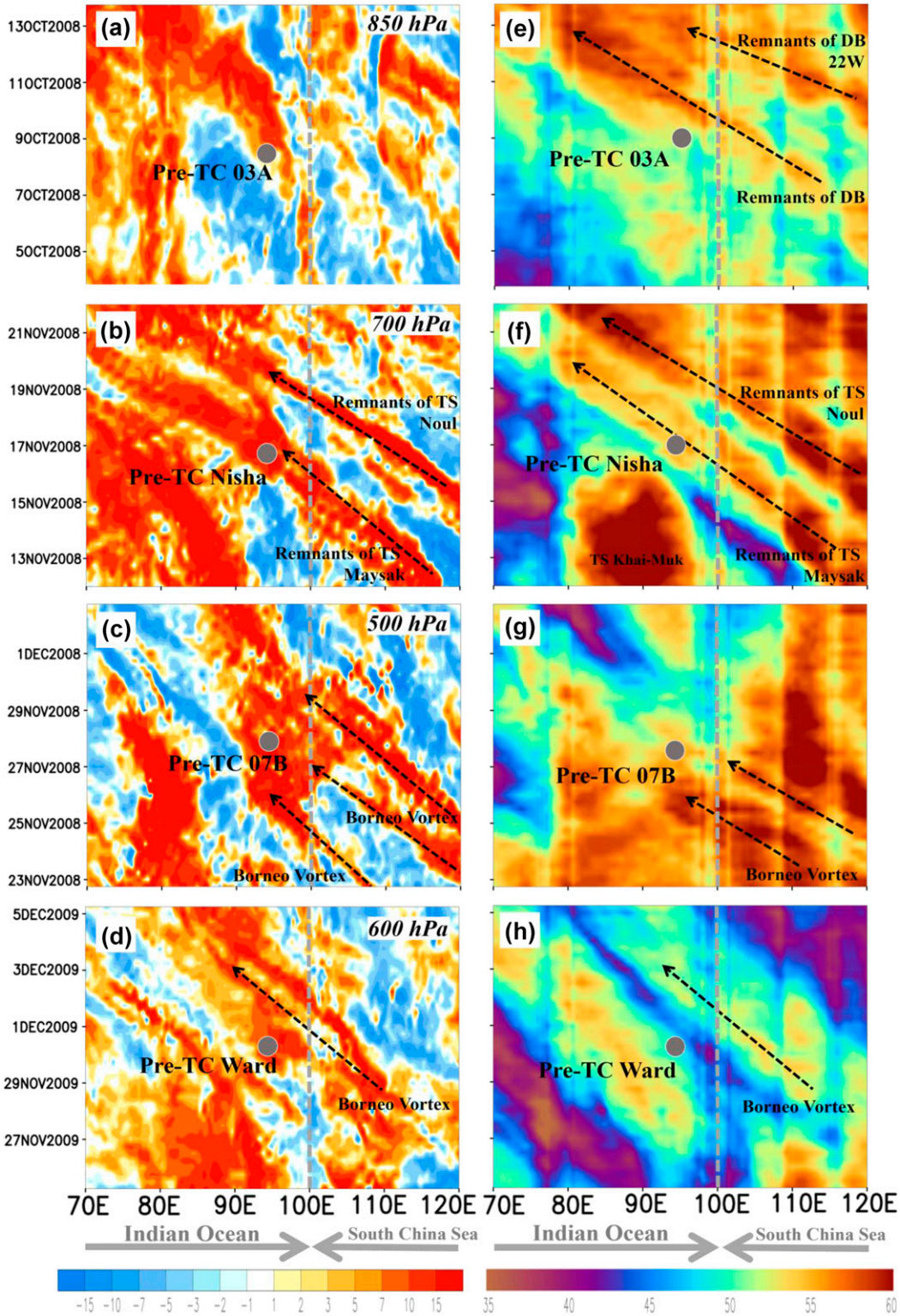

FIG. 4. Longitude–time (Hovmöller) diagrams of mean (a)–(d) relative vorticity ($10^{-5}\,s^{-1}$) at the pressure level as labeled (same as in Fig. 3) and (e)–(h) total column-integrated precipitable water (mm) in ECMWF-YOTC data during the case period of 03A, Nisha, 07B, and Ward, respectively (from top to bottom). The latitudinal range of averaging is 0°–15°N. The circles depict the time of lee vortex formation, a disturbance is depicted as "DB," and the vertical dashed lines near 100°E mark the boundary between the IO and the SCS.

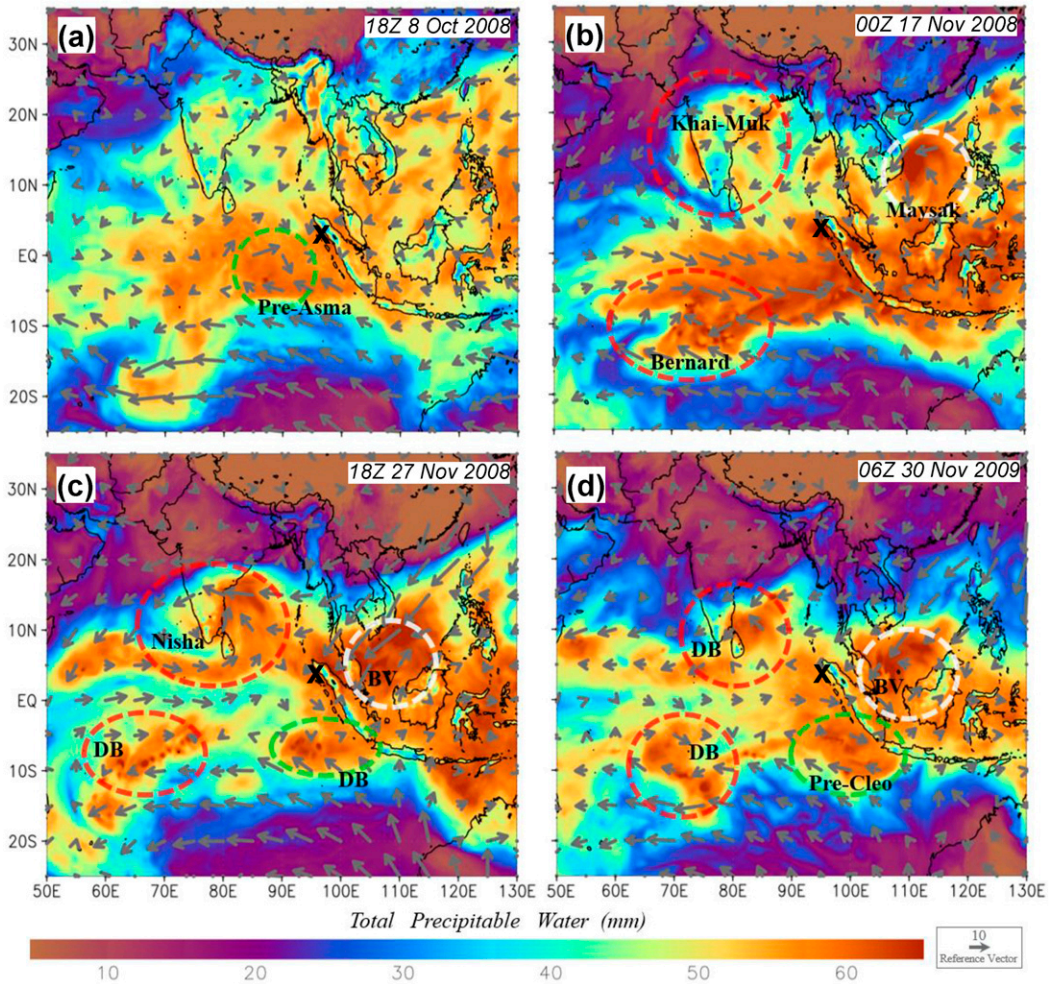

FIG. 5. Distribution of total column-integrated precipitable water (mm, color) and horizontal wind at 925 hPa ($m\,s^{-1}$, gray vectors) at the time of lee vortex formation for (a) 03A, (b) Nisha, (c) 07B, and (d) Ward, respectively. The vortex centers (at 850 hPa) are marked by an "×." The red dashed circles depict TC or disturbance (DB) in the IO, green dashed circles depict TD or pre-TC in SIO, and white dashed circles depict BV or TC remnant in the SCS. Both the reference vector and color scales are plotted at the bottom.

remnants of TS Maysak for Nisha, while there are possibly some linkages with the remnants of a tropical depression for 03A, and a BV for both 07B and Ward, respectively. These precursor systems also carried a higher moisture content (in total precipitable water) into the lee area or its vicinity (Fig. 4, right column). For the latter two cases, the vorticity associated with the incipient BV was stronger with a wider circulation (Figs. 3c,d) and maximized farther aloft near 500–600 hPa around t_0 (Figs. 2c,d). As the vortex moved downstream afterward, it developed downward toward the surface and the low-level ζ strengthened (Fig. 2). Apparently, these migratory synoptic disturbances provided incipient vorticity and moisture and were also helpful to the development of lee vortex, and subsequently the TC at a later time (e.g., Gray 1968).

Figure 5 presents the 925-hPa flow fields and precipitable water amount in a larger domain at t_0 for the four NIO cases. Except for 03A, which had a weaker flow, strong northeasterly or northerly winds from cold air surges from midlatitudes were present over much of the SCS and Malay Peninsula in the other three cases (Figs. 5b–d). The relatively dry cold air became easterly as it traveled south and reached the northern tip of Sumatra at this time. Meanwhile, along the equator, there existed a westerly wind burst (WWB) of 5–20 $m\,s^{-1}$ at low levels in these three cases. Interestingly, a pair of synoptic-scale vortices were also present across the equator in the IO (red dashed circles in Fig. 5) in each case, and their circulations (with enhanced horizontal pressure gradients) possibly

helped the equatorial westerlies to intensify, in a way previously pointed out by Lee et al. (1989).

In all four cases, low-level southeasterly flow prevailed over a vast area south and southwest of Sumatra (Fig. 5). Coupled with the westerly flow (or a weaker flow) along the equator, this provided cyclonic vorticity (in the Southern Hemisphere) for the region west of southern Sumatra, as shown in Figs. 5a, 5c, and 5d (green dashed circles), also consistent with Lee et al. (1989) and Fine et al. (2016, their Fig. 7). The vortex west of southern Sumatra in Fig. 5d later developed into Cleo, which formed a vortex pair with Ward. As mentioned, the remnants of western Pacific tropical disturbances or BVs were associated with higher moisture content in the SCS (white dashed circles in Fig. 5) at this time (for Nisha, 07B, and Ward), and would soon move into the lee side of northern Sumatra.

Thus, some common precursor synoptic-scale features or ingredients can be identified from Figs. 3–5 for the four TC cases in NIO. They include low-level northeasterly wind surges in the SCS, WWBs along the equator to the west of Sumatra, and an incipient disturbance that brought stronger relative vorticity and higher moisture content into the lee area through horizontal advection. Among these features, the equatorial westerly winds were most likely also enhanced by vortex pairs across the equator when they developed. Below, the two stronger cases that became named storms [i.e., TS Nisha (2008) and TC Ward (2009)] are further selected for numerical simulation and an investigation to assess the relative importance of the topography of Sumatra, in particular to the subsequent TC formation. To achieve this goal, both CTL and NT experiments were performed for each case, and their results are compared in the following section.

4. Model results of Nisha and Ward in the northern Indian Ocean

a. Tropical Storm Nisha (2008)

For each case, the CTL experiment needs to be validated against the observations to ensure that the event is reproduced reasonably well. First, the modeled track and intensity for Nisha (2008) are shown in Fig. 6. Overall, the simulated track is fairly close to the track in the YOTC data, and the vortex first forms at the lee side of northern Sumatra and then moves westward and northwestward toward Sri Lanka and southern India, despite some discernible differences (Fig. 6a). In particular, the landfall points in Sri Lanka and southeastern India in CTL are quite close to the observation, an encouraging result for a model run 15 days in length. Similarly, reasonable results are obtained by the model for the intensity of Nisha (Fig. 6b). In CTL, the timing to reach TS intensity (34 kt) is only about 1.5 days earlier than the JTWC data, while the modeled peak intensity (54 kt) on 26 November is also very close to the best track (50 kt). A deficit of about 10 hPa in the TC's minimum mean sea level pressure (MSLP) appears after Nisha reached TS status, when the JTWC best track suggested 985 hPa (Fig. 6c). Thus, the central MSLP in CTL is only about 5–10 hPa lower than the YOTC data, but the peak wind speed is considerably stronger (by nearly 20 kt) and close to the JTWC data due to the high resolution of the model. At early stages before TS, the maximum wind speed in CTL is also consistently stronger than the YOTC. Overall, the simulation in track and intensity for Nisha is quite reasonable.

In Fig. 7, the model outputs of the column-maximum mixing ratio of precipitation (rain, snow, plus graupel) and low-level winds (at 1547 m) are compared to the SSM/I brightness temperature for deep convection and rainband structure of TS Nisha and the YOTC winds at 850 hPa, at selected times of similar evolutionary stage. Even though the two quantities for convection are not identical, the figure provides verification that the model well reproduced the storm structure of Nisha before and during its TS stage since 23 November. For example, the convection was quite loose and more scattered when the storm first approached Sri Lanka (Figs. 7a,e), became more organized but asymmetrical (more in the northern quadrants) on 24 November (Figs. 7b,f), then further tightened in cloud structure on the approach to southern India (Figs. 7c,d and g,h). Overall, the simulation agrees very well with the observation in cloud patterns and low-level circulation.

The time–height section (0–12.3 km) of ζ for the vortex in CTL, also averaged inside 550 km from the center, is presented in Fig. 8a and can be compared with Fig. 2b from the YOTC data for their general characteristics. Overall, the two plots are similar in both the magnitude and vertical structure of the areal-mean ζ, but some differences still exist. For example, the model vortex appears weaker than that in the ECMWF-YOTC analyses in the lower levels during its leeside stage, but not so when one compares peak wind speed or central MSLP (cf. Fig. 6). After the vortex starts to shed, the CTL result agrees closely with the ECMWF in areal-mean ζ (Figs. 2b, 8a), and Nisha in CTL reaches TS intensity at 0000 UTC 24 November, roughly 42 h before the time issued by JTWC (Fig. 6b) as mentioned.

When the terrain of Sumatra is removed in the NT experiment, the simulated track remains close to that in CTL (Fig. 6a). At first glance, the time–height ζ inside

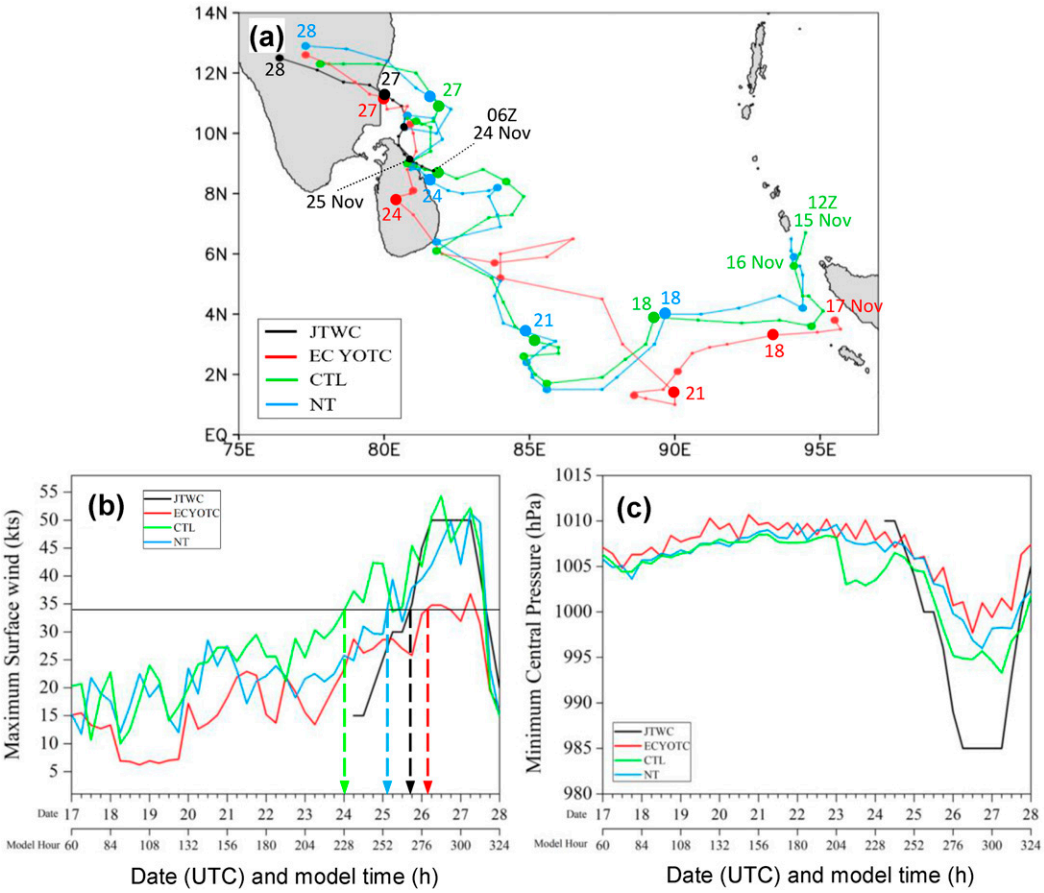

FIG. 6. Comparison of (a) track, (b) maximum surface wind speed (kt, at 10 m above the surface), and (c) central mean sea level pressure (hPa) among JTWC best track, ECMWF-YOTC, and CTL and NT experiments for the case of Nisha (16–28 Nov 2008). The vortex center positions (at or near 850 hPa) are given by small dots every 6 h, median dots at 0000 UTC, and large dots every three days with dates labeled (unless not necessary) in (a). Track endpoints are also labeled (with time if not at 0000 UTC). In (b), TS intensity (34 kt) and the time to reach it in the four data sources are marked.

550 km for Nisha in the two runs also appear similar, including the lee stage (Figs. 8a,b). Their differences, many quite subtle, can be better depicted in Fig. 8c (CTL minus NT), where the areal-mean ζ at low levels in CTL tends to be stronger than that in NT for much of the time since 17 November, especially over 21–26 November as the vortex strengthens to reach the TS status. In agreement with Fig. 8c, the near-surface flows (below 1 km) in CTL also produce a stronger vorticity belt and a clearer vortex circulation center on 21 November (figure not shown). This result is consistent with Epifanio and Durran (2001), who suggest that topography can form corner flow and provide stronger shear vorticity to the downstream area. With a weaker mean ζ, the maximum wind speed associated with Nisha in NT is weaker than that in CTL over 21–27 November (Fig. 6b), often by 5–10 kt, and the storm reaches TS intensity on 25 November, more than one day (27 h) later than in CTL. Even though the storm in CTL is stronger through much of its lifespan (Figs. 6b,c), the one in NT also reaches TS status when the topography of Sumatra is removed.

To gain insight into the development of the lee vortex in CTL and to contrast it with the one in NT, a vorticity budget analysis (cf. section 2c) is performed on the vortex at a height of 1547 m (near 850 hPa), averaged also inside a radius of 550 km from the center, for its lee stage as shown in Fig. 9. For the pre-Nisha lee vortex in CTL (1200 UTC 15 November–0000 UTC 18 November 2008, t = 24–84 h), it is seen that the mean ζ at 1547 m (dashed curve with dots) generally increases with time during this 60-h period, roughly from 0.8 to 1.7 $\times$ $10^{-5}\,s^{-1}$ (Fig. 9a), mainly contributed by two terms: convergence/stretching (green) and vertical advection (brown). The convergence effect is counteracted (out of phase) by horizontal advection (blue) as the same low-level inflow also tends to bring in lower ζ values from

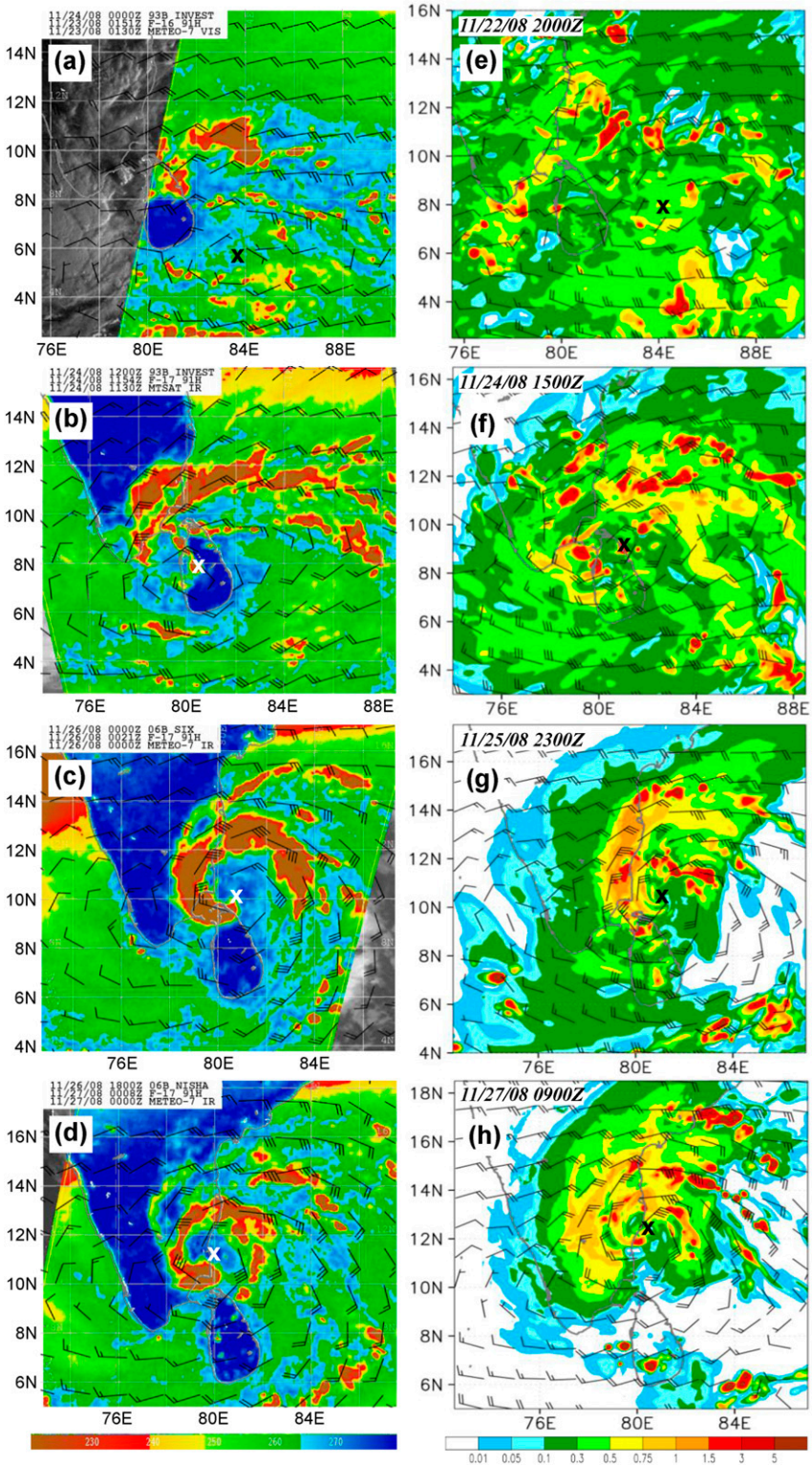

FIG. 7. (a)–(d) SSM/I 91-GHz imagery of brightness temperature (T_B, K, color) of Nisha at (a) 0151 UTC 23 Nov, (b) 1154 UTC 24 Nov, (c) 0021 UTC 26 Nov, and (d) 0008 UTC 27 Nov 2008 (source: NRL), overlaid with ECMWF-YOTC wind fields (kt, 1 full barb = 10 kt) at 850 hPa at the closest time with data (every 6 h). (e)–(h) Column maximum mixing ratio of precipition (g kg^{-1}, rain + snow + graupel) and horizontal wind at 1547 m (kt) in CTL at (e) 2000 UTC 22 Nov, (f) 1500 UTC 24 Nov, (g) 2300 UTC 25 Nov, and (h) 0900 UTC 27 Nov, respectively. The color scales are plotted at the bottom, and the storm center is marked by an "×."

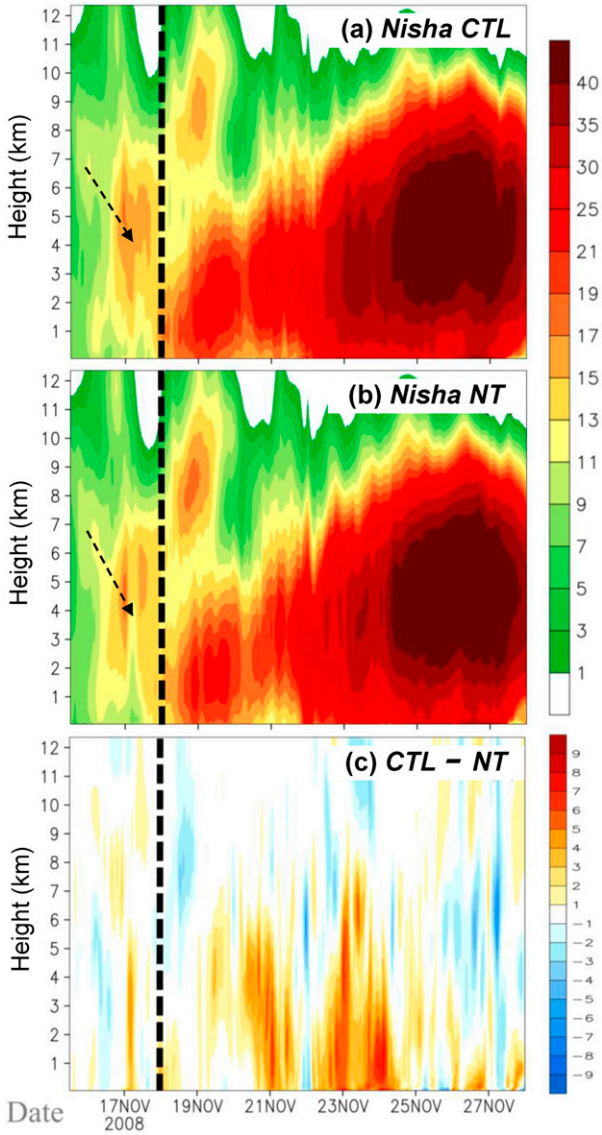

FIG. 8. Time–height section of mean relative vorticity (ζ, $10^{-6}\,s^{-1}$) for Nisha similar to Fig. 2b, except from (a) CTL and (b) NT experiment, and (c) their difference (CTL − NT). Downward developments during the lee stage are marked.

larger radii, while the vertical advection is largely cancelled by the tilting term (red) since the stronger upward motion at the vortex center also tilts the vorticity vector from the vertical (rotation on x–y plane) into horizontal direction (rotation on vertical plane). While all the above four terms reach around $2 \times 10^{-9}\,s^{-2}$ in their peak magnitude, the friction/residual term is significantly smaller and the solenoidal effect is negligible. As a result, the local tendency of ζ in Fig. 9a (computed using time differentiation) is a relatively small net difference among the larger rhs terms with opposite signs, but is mostly positive to cause the gradual increase in ζ. During 16 November, the areal-mean w at 1547 m is in fact slightly negative (figure not shown) and indicates leeside sinking and stretching (Fig. 9a). After 0600 UTC 17 November, on the other hand, mean w turns positive with growth in ζ near 1 km (Fig. 8a), as the vortex gradually moves away from the terrain (cf. Fig. 6a). While the budget results exhibit similar characteristics in the NT run (Fig. 9b), the convergence and vertical advection terms are often smaller than in CTL, yielding a mean ζ (at 1547 m) of roughly $1.4 \times 10^{-5}\,s^{-1}$ at 0000 UTC 18 November. On 17 November when the mean ζ starts to show larger deficit (cf. Fig. 8c), such differences in budget terms are also more evident. The increase in both the convergence and vertical advection terms in CTL on 17 November indicate that the two effects work in phase. In short, the results from Figs. 8 and 9 suggest that the Sumatra topography is helpful to produce a stronger pre-Nisha vortex at the lee side, and most likely as a result, Nisha reaches the TS status 27 h earlier in CTL compared to its counterpart in NT.

As reviewed in section 1, the blocking effect of Sumatra on the northeasterly flow can be characterized by Fr, and a larger (smaller) value favors the flow-over (flow-around) regime. Here, h is set to 1895 m obtained for northern Sumatra, and the mean U and N values (time variant) at 3°–7°N along 100°E below 2 km (cf. Fig. 1a) are used following Fine et al. (2016). To reveal possible influence of Fr on vorticity generation at the lee side, the correlation coefficients between Fr and lagged mean vorticity tendency at 1547 m (as in Fig. 9) from hourly data are computed and presented in Fig. 10a for the pre-Nisha vortex. In CTL, the coefficient (green curve) is positive and at least ~0.2 for all lag time within 24 h, but is higher over 18–24 h with a peak value of 0.46. While these values are not high (since Fr is only one of the factors), this result indicates that a strengthening in the low-level prevailing northeasterly flow generally helps to increase the leeside vorticity, and its influence is quite persistent. Without the terrain in NT (U and N are different from those in CTL, but h is still set to 1895 m for consistency), on the other hand, the enhancement in northeasterly flow can contribute more directly to the lee vortex, as the coefficient peaks at 0.69 at a lag time of only 3 h and remains >0.5 within 7 h. However, the coefficient drops rapidly after 11 h (Fig. 10a), so the influence does not last long.

b. *Tropical Storm Ward (2009)*

For TS Ward (2009), the observed and modeled track and intensity are presented in Fig. 11. All four tracks (JTWC, ECMWF-YOTC, and the two model runs CTL and NT) are close to one another, with movement generally toward the west during 3–9 December and then

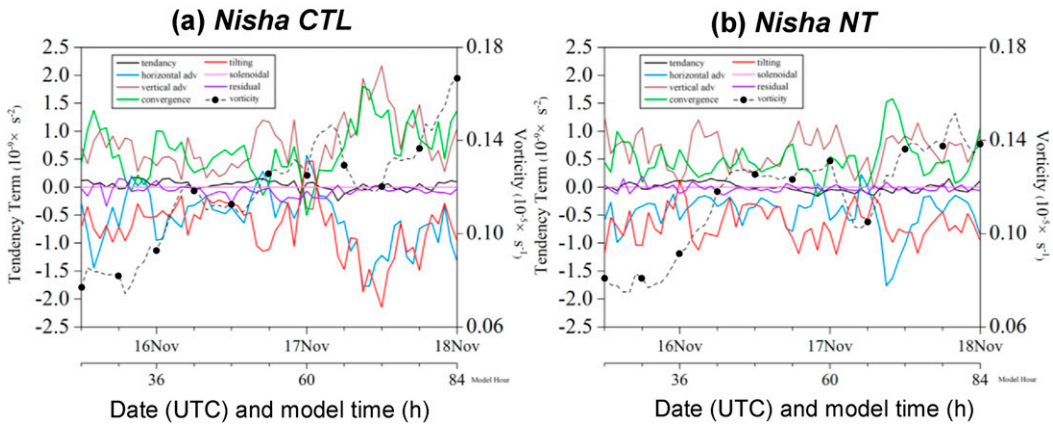

FIG. 9. The vorticity-tendency budget terms ($10^{-9}\,s^{-2}$, left axis), including local tendency, horizontal advection, vertical advection, convergence, tilting, solenoidal, and residual terms (see legend), and the mean vorticity ($10^{-5}\,s^{-1}$, dashed with dots, right axis) at the height of 1547 m, averaged inside 550 km, for Nisha from 1200 UTC 15 Nov to 0000 UTC 18 Nov 2008 in (a) CTL and (b) NT experiment.

toward the north during 9–12 December afterward (Fig. 11a). As in JTWC, the storms eventually make landfall in central Sri Lanka from the east, though with some variations in timing. The landfall time in ECMWF data is near 1800 UTC 12 December and about 40 h earlier than that in JTWC (1200 UTC 14 December), and a similar early landfall also occurs in the two CReSS experiments, near 1500 UTC in CTL and 1800 UTC in NT on 12 December. Again, at a range of nearly two weeks, such track errors (about 200 km) in Fig. 11a are in fact very small. Before landfall, all four data give almost identical timing, within a 6-h period, to reach the TS status on 11 December (Fig. 11b). The two simulations produce a maximum surface wind speed stronger than JTWC best track, but the intensity quickly drops after 12 December (especially in CTL) due to the early landfall. Most likely for the same reason, the central MSLP in the model runs over 12–13 December are also not as low as that in JTWC (Fig. 11c), as they are closer to Sri Lanka than the observation. During 6–9 December when the pre-Ward vortex tracks westward, nevertheless, its intensity in CTL tends to be stronger compared to NT (Fig. 11b).

For the period since 6 December, the storm rainfall structure and low-level circulation of Ward in CTL are compared with SSM/I satellite observation and YOTC data in Fig. 12. Similar to the Nisha case, the model successfully captures the general characteristics of rainfall structure, its asymmetry, and time evolution. As the storm tracked toward Sri Lanka in the NIO on 6 December, the convection was loose and farther away from the center (Figs. 12a,d). During 9–12 December as the storm strengthened to reach TS (cf. Fig. 11b), it became tighter in cloud structure (Figs. 12b,e), and developed in a clear comma cloud shape to the east of the storm center on 11–12 December (Figs. 12c,f). However, this structure

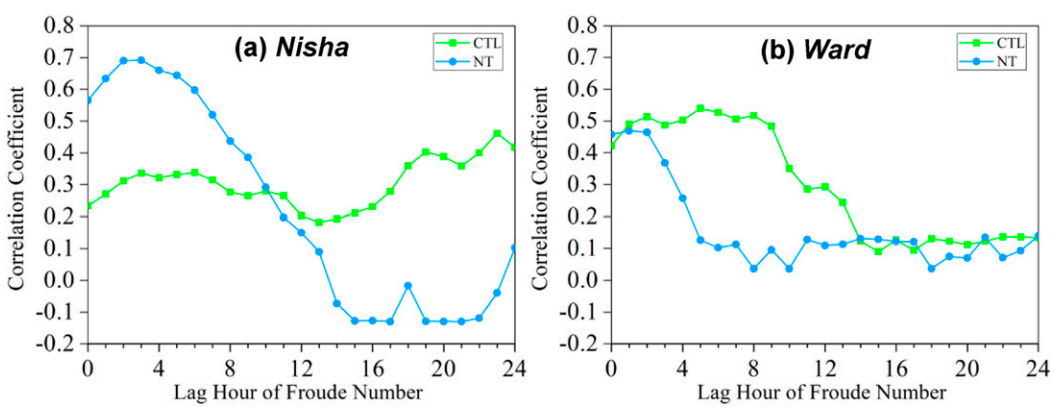

FIG. 10. The correlation coefficients between Fr and lagged mean vorticity tendency (as in Figs. 9, 14), as a function of lagged time (h) in CTL and NT experiments for the case of (a) Nisha and (b) Ward, respectively.

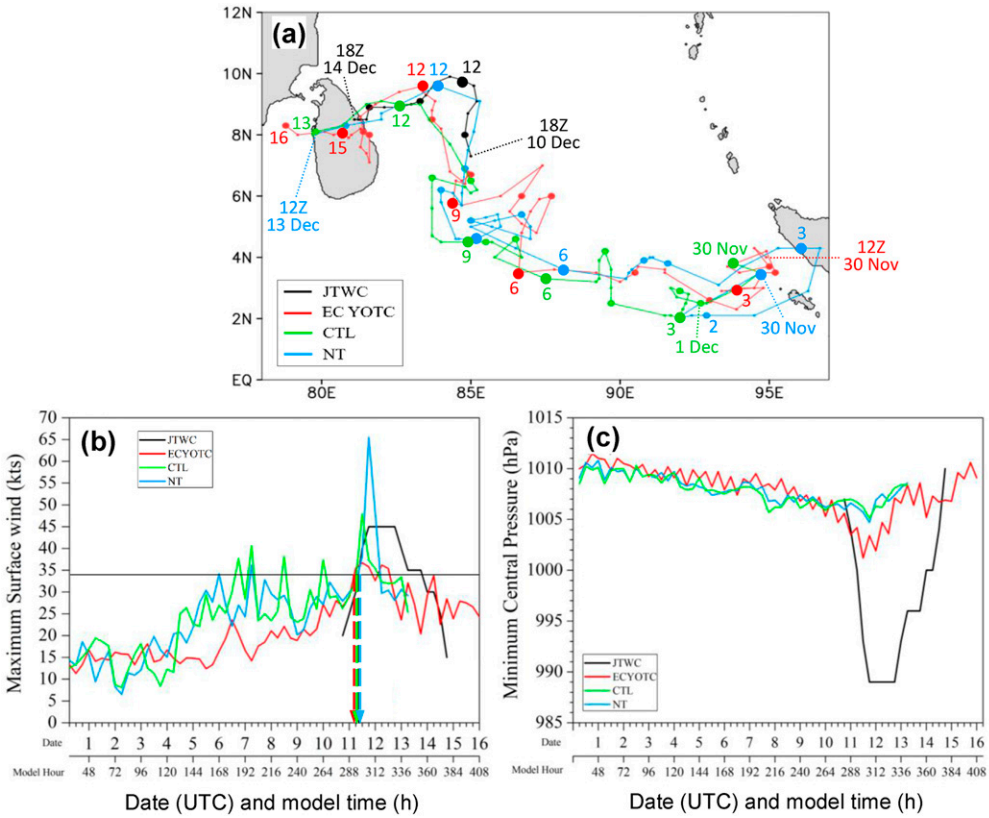

FIG. 11. As in Fig. 6, but for the case of TC Ward (30 Nov–16 Dec 2009).

deteriorated afterward as the storm moved closer to land (not shown).

The time–height plot of areal-mean ζ inside the radius of 550 km in CTL for the vortex in the case of Ward, as shown in Fig. 13a, agree reasonably well with that constructed from ECMWF-YOTC analyses (cf. Fig. 2d), and both are weaker and do not extend upward as deep compared to the Nisha case (cf. Figs. 2b, 8a). Again, the time–height structure of ζ in NT (Fig. 13b) is very close to CTL, and there is a tendency for downward development of ζ in the lee stage in both runs, from about 5 km toward the lower levels. While close, Fig. 13c still reveals that the vortex in CTL is stronger than that in NT during most of the lee stage that ends at 0000 UTC 4 December, except for a brief period around 0000 UTC 3 December. This difference in lee vortex strength is more pronounced than the Nisha case (cf. Fig. 8c). However, such an advantage of CTL over NT does not maintain throughout the life span of Ward, and the storm in CTL reaches TS intensity only 4 h earlier (Fig. 11b).

The areal-mean vorticity budget (550 km from center) at 1547 m for the pre-Ward lee vortex (t = 24–96 h) in CTL (Fig. 14a) shows that the mean ζ is generally above $1.2 \times 10^{-5}\,\mathrm{s}^{-1}$ from 1800 UTC 30 November to 1200 UTC 2 December and mainly contributed by the convergence/stretching term (green), which is again largely cancelled by horizontal advection. In this case, the vertical advection term (brown) can be either positive or negative in different time periods but remains out of phase from the tilting effect (red), which therefore also contributes toward ζ from time to time (when negative vertical advection occurs). In periods when the areal-mean w at 1547 m is negative (e.g., first half on 1 December, not shown), this leeside sinking (with downward acceleration) is accompanied by positive convergence and vertical stretching effect (Fig. 14a). In NT, the ζ-budget calculation reveals similar results to CTL (Fig. 14b), but the contribution from convergence is generally smaller and the mean ζ grows to exceed $1.2 \times 10^{-5}\,\mathrm{s}^{-1}$ only toward the end, after about 1200 UTC 2 December. This is because a BV (visible in Figs. 3d, 4d, and 5d) is moving across the northern Sumatra (near 97°E) from upstream around this time, and without Sumatra's terrain, the lee vortex in NT moves eastward to merge with the BV (Fig. 11a), resulting in an increase in mean ζ and a stronger vortex in NT (versus CTL) near 3 December (Fig. 14). In contrast,

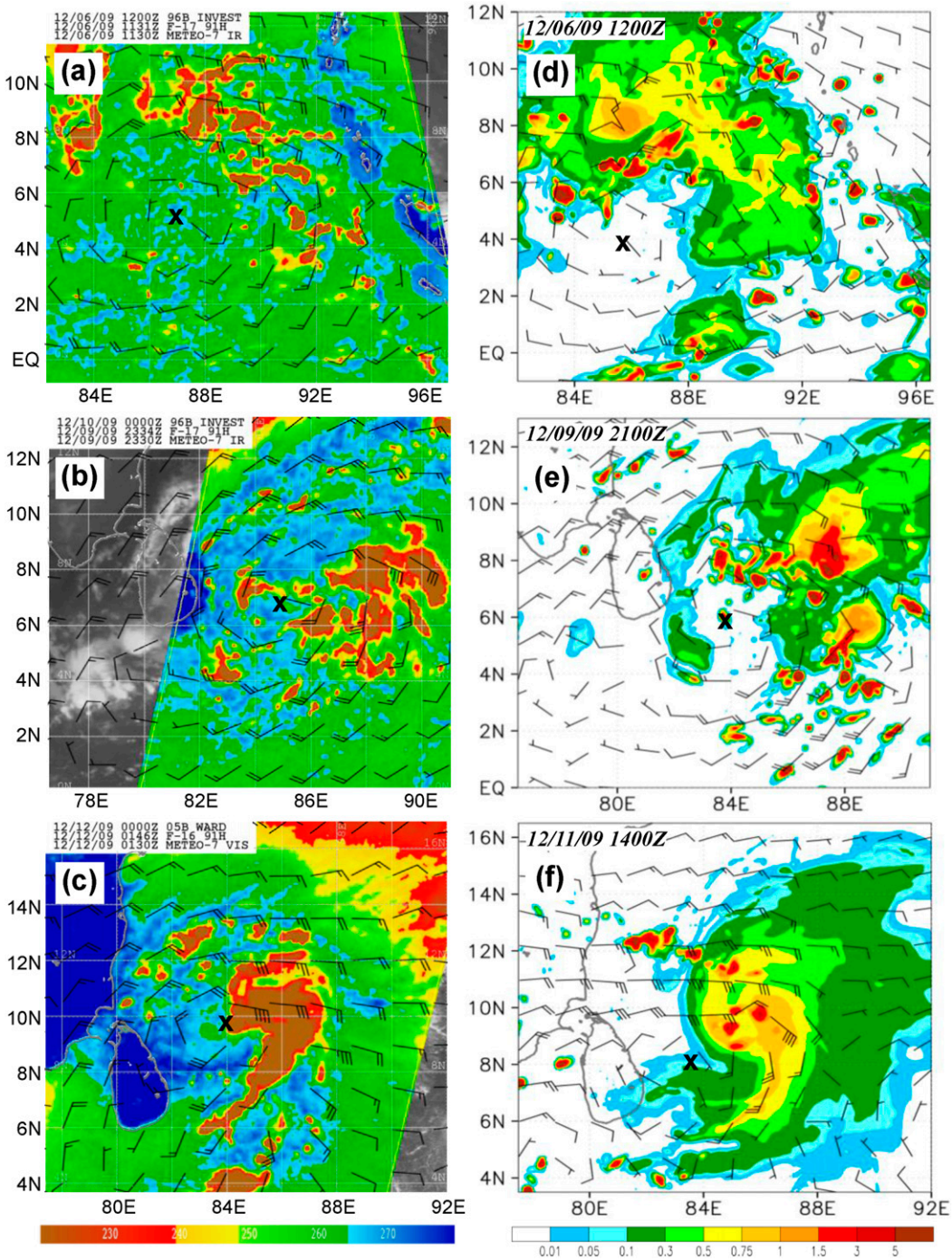

FIG. 12. As in Fig. 7, but for Ward at (a) 1130 UTC 6 Dec, (b) 2334 UTC 9 Dec, and (c) 0146 UTC 12 Dec 2009 (source of satellite imagery: NRL), and (d) 1200 UTC 6 Dec, (e) 2100 UTC 9 Dec, and (f) 1400 UTC 12 Dec from CTL at a similar stage as in (a)–(c), respectively.

with topography, the lee vortex in CTL remains stationary near 3 December, and a direct merger does not occur (Fig. 11a).

The results of lagged correlation between upstream Fr and areal-mean ζ at 1547 m at the lee side (east of 90°E and before 0600 UTC 2 December to exclude the influence from the BV) indicate that for the pre-Ward lee vortex, the coefficient (green) in CTL remains high within about 10 h and peaks at 0.54 with a 5-h lag time (Fig. 10b). In contrast, the coefficient drops rapidly after

only 3 h in NT, from a maximum of 0.47 at 1 h. Thus, in both Nisha and Ward, the terrain tends to exert a longer, more persistent influence on the generation of leeside vorticity (through either subsidence warming or corner effect, or both) in CTL experiments, in comparison to NT runs where ζ is provided only through horizontal advection and/or shearing effect and for a shorter duration.

5. Model results of Cleo in the southern Indian Ocean

During the same period as Ward, another vortex also evolved into Cyclone Cleo in SIO as mentioned, so the same simulations (CTL and NT) are used to discuss its development as well here. Since the equatorial westerlies were present leading to the formation of this closed vortex to the west of southern Sumatra/western Java (Fig. 3d), the pre-Cleo vortex is not a lee vortex as pointed out by Fine et al. (2016). After formation, pre-Cleo first remained stationary for a few days, then moved toward the west-southwest quite steadily after 3 December (Fig. 15a). In CTL and NT, the corresponding vortices both form at the same location and time (at 0000 UTC 29 November) as the YOTC analysis, and also have a similar track. However, compared to analysis, the vortex in CTL starts to move westward (near 0600 UTC 3 December) about 12–18 h too late, and even more so in NT (Fig. 15a). Later in the simulations after 1200 UTC 8 December, all tracks converge toward the JTWC with reduced track errors.

The JTWC best track data indicate that Cleo reached TS intensity near 0000 UTC 7 December (Fig. 15b) but this occurs roughly 24 h later in CTL, and another 12 h later in NT, whose vortex moves out from its formation area the latest, as mentioned. Both vortices, nonetheless, reach 34 kt at an earlier time but only briefly. After 1200 UTC 7 December, TC Cleo underwent a period of rapid intensification to reach a peak wind speed of over 110 kt and a central MSLP of lower than 940 hPa (Figs. 15b,c). In the model, however, the storm is gradually approaching the domain boundary during this period (cf. Fig. 1b) and a similar intensification does not take place. Although not ideal, this is acceptable since our focus is on the formation and earlier stages of the vortex. For selected times during 3–7 December, Cleo's rainfall structure in CTL is also compared with satellite observations, and the two are similar and in good agreement, including the asymmetry and evolutionary characteristics (Fig. 16).

The time–height cross sections of areal-mean ζ (inside 550 km) of the pre-Cleo vortex are again similar in CTL and NT runs (Fig. 17), where a downward development

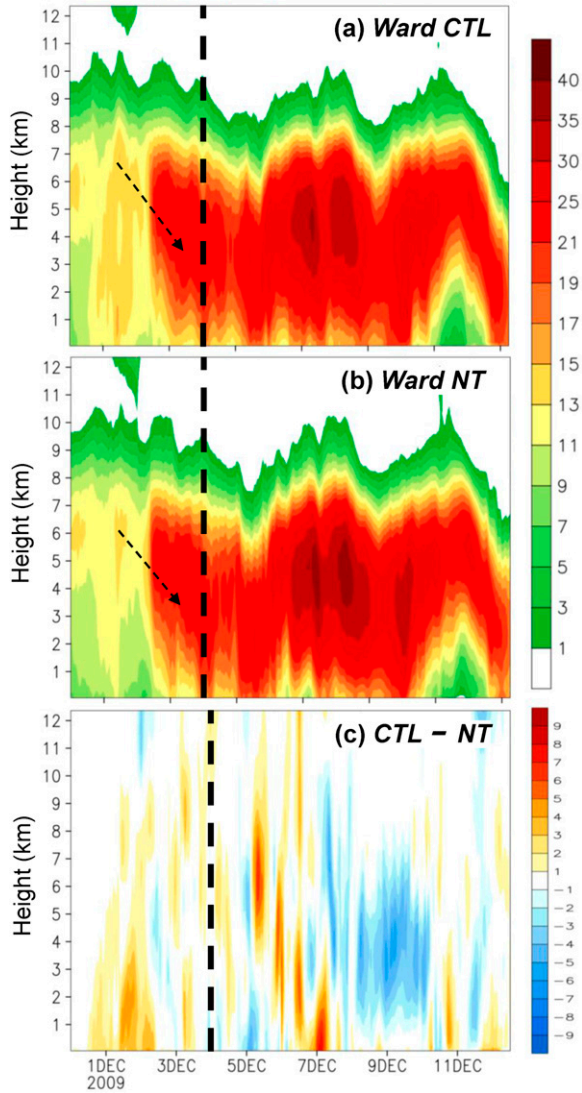

FIG. 13. As in Fig. 8, but for the case of TC Ward.

of ζ with time is evident before 5 December. In Fig. 17c, one can also see that the vortex in CTL is persistently stronger and extends deeper into the upper troposphere than that in NT during the stationary stage closer to Sumatra, but not so at low levels after 4–5 December. This latter difference, however, mainly exists only over outer regions at larger radii, as the peak 10-m wind at the inner core remains clearly stronger in CTL over 5–8 December (cf. Fig. 15b).

Prior to 0000 UTC 4 December (t = 48–120 h), the generation of mean vorticity is again mainly from convergence/stretching and vertical advection terms (Fig. 18), which also tend to be greater in CTL than those in NT. In Fig. 19, the low-level mean winds below 2 km over the northeastern quadrant of the vortex (also

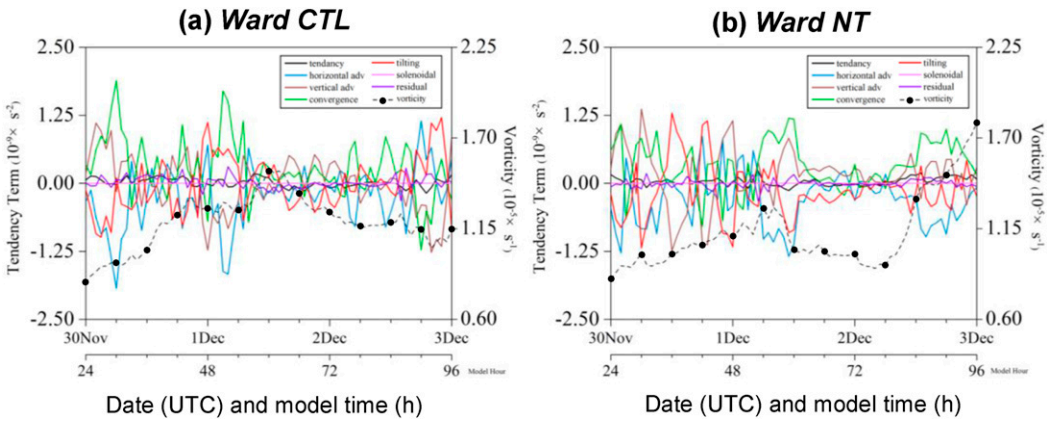

FIG. 14. As in Fig. 9, but for Ward from 0000 UTC 30 Nov to 0000 UTC 3 Dec 2009.

within 550 km) in the two experiments are compared. Without the topography, the mean wind is between westerly and west-northwesterly in NT, but persistently northwesterly in CTL. Thus, the Sumatra Island acts to block the equatorial westerly flow to provide a larger southward component and stronger curvature vorticity at low levels. This result is consistent with Fine et al. (2016), who speculated that the topography of Sumatra

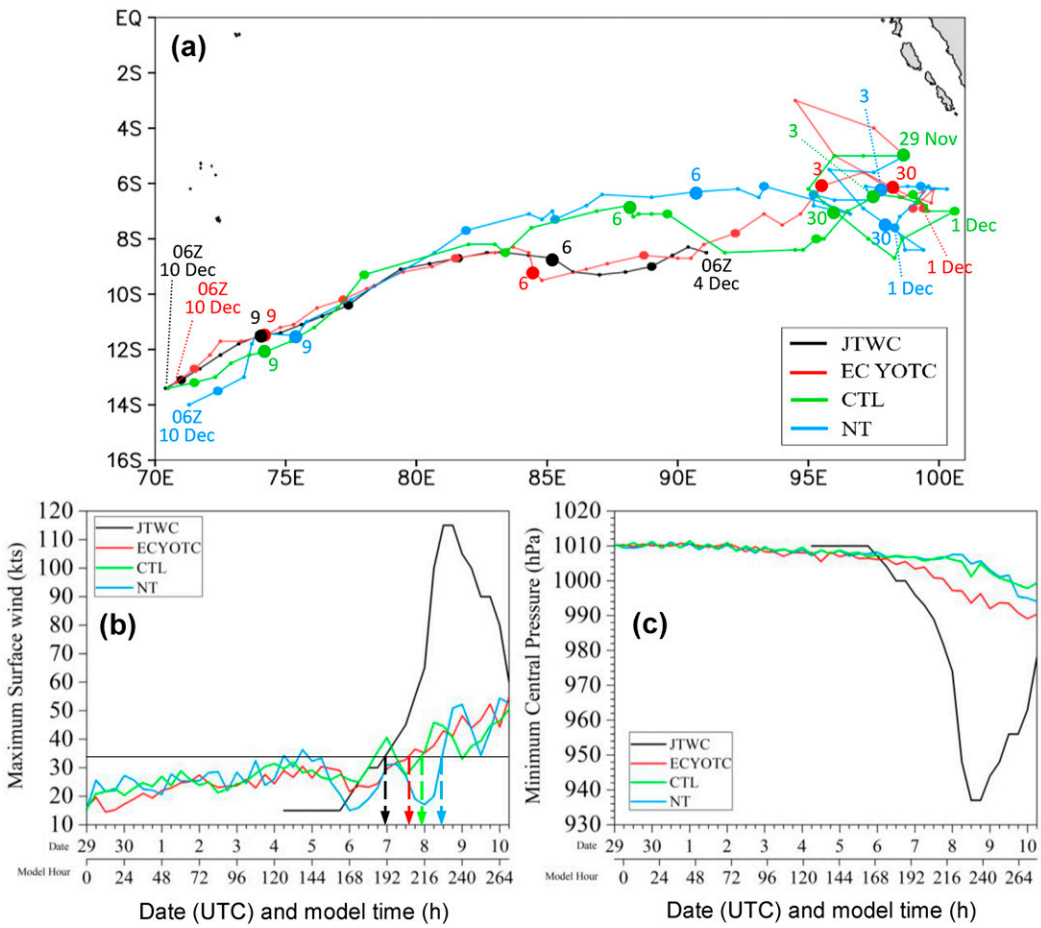

FIG. 15. As in Fig. 6, but for the case of TC Cleo (29 Nov–10 Dec 2009).

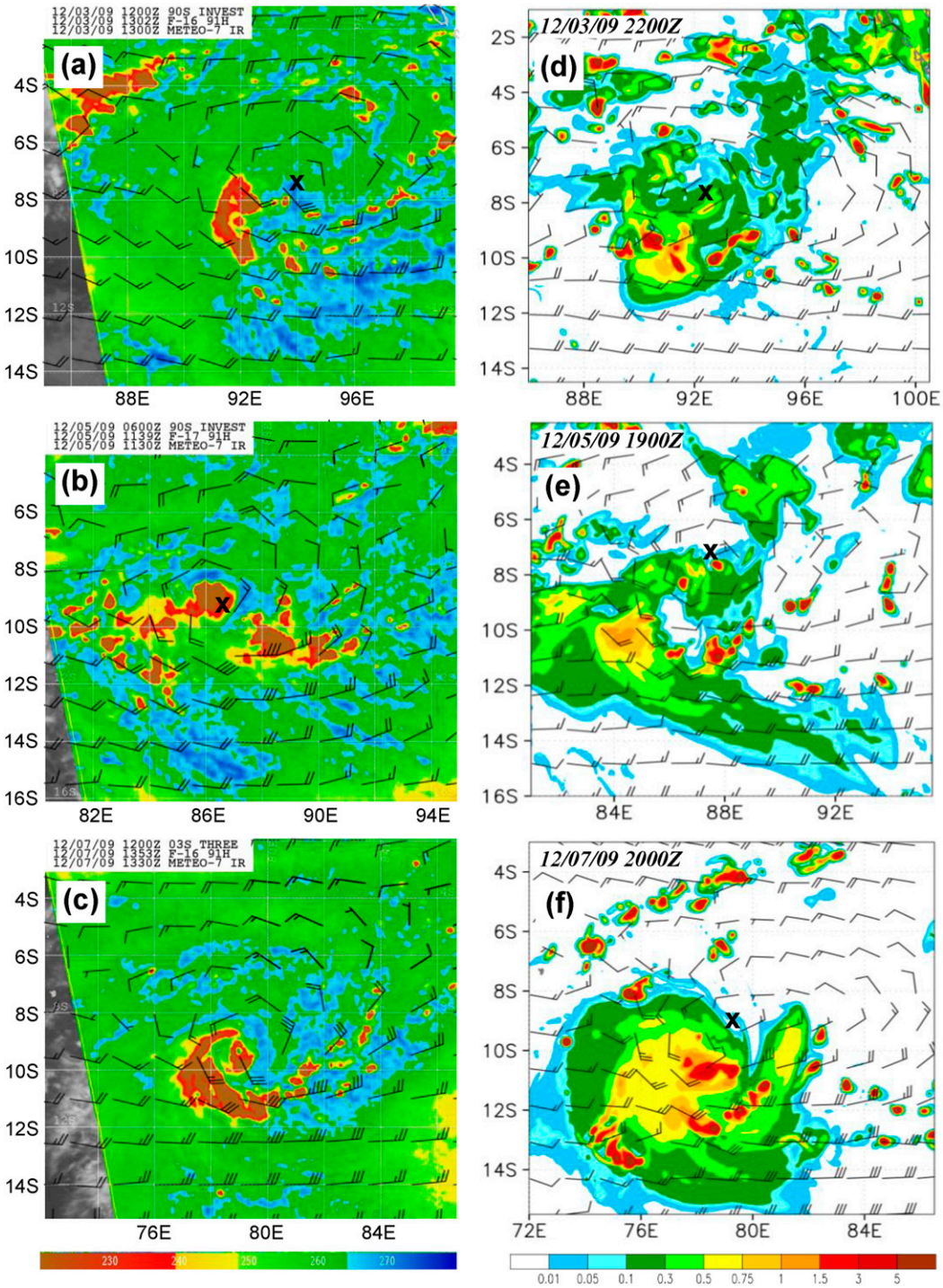

FIG. 16. As in Fig. 7, but for Cleo at (a) 1302 UTC 3 Dec, (b) 1139 UTC 5 Dec, and (c) 1353 UTC 7 Dec 2009 (source of satellite imagery: NRL), and (d) 2200 UTC 3 Dec, (e) 1900 UTC 5 Dec, and (f) 2000 UTC 7 Dec from CTL at a similar stage as in (a)–(c), respectively. The storm center in (c) is not marked for clarity.

helps the vortex of pre-Cleo to gain strength. Thus, in the case of Cleo (2009) where its initial vortex is not at the lee side, the blocking effect of southern Sumatra on the equatorial westerlies, nevertheless, helps to provide stronger curvature vorticity and leads to a stronger, tighter and more compact vortex during it westward movement. Eventually, the storm in CTL reaches the TS status 12 h before that in NT (Fig. 15b).

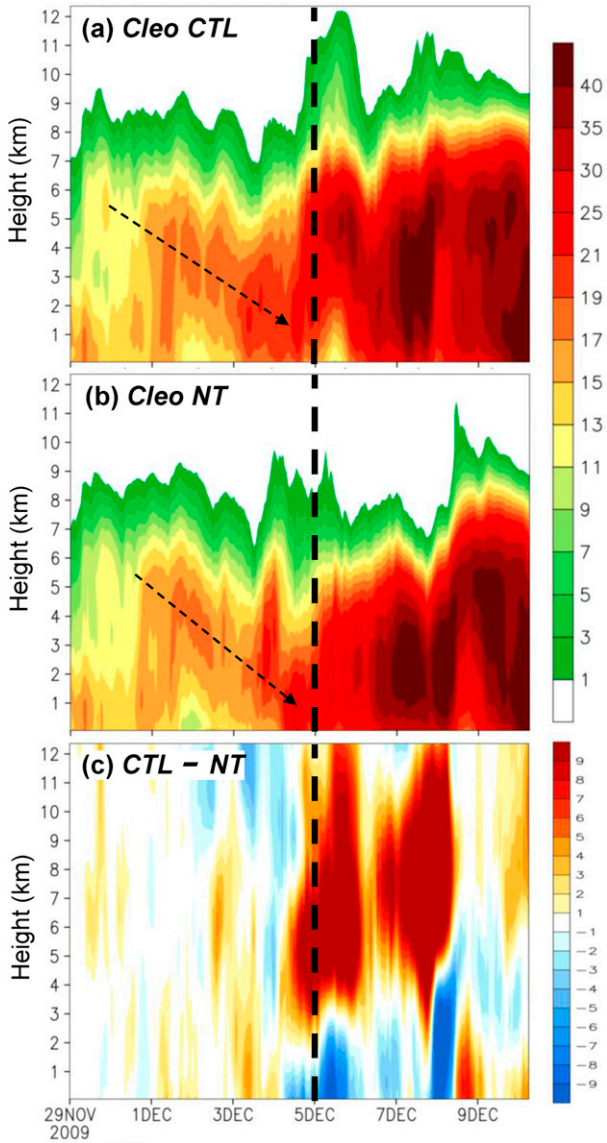

FIG. 17. As in Fig. 8, but for the case of TC Cleo.

6. Discussion

In the CTL experiments, the two lee vortices in NIO (Nisha and Ward) tend to be stronger during the majority of the lee stage (Figs. 8, 13) and subsequently reach the TS status earlier compared to their counterpart in NT runs (Fig. 6b), although the difference is small and perhaps not significant for Ward (Fig. 11b). Despite this, however, the storms in NT runs form in approximately the same location and reach TS status (although more slowly) without the topography of Sumatra. Even if a different criterion for TC formation (e.g., 25 kt) is adopted, the results are similar (cf. Figs. 6b, 11b). Thus, for the cases simulated here, our results indicate that the island of Sumatra is only a beneficial factor rather than a necessary condition for the formation of TCs (typically several days later). This conclusion should not come as a surprise since the majority of named TCs in NIO do not originate from the lee side of Sumatra (e.g., Fine et al. 2016). It follows that some other factors common in both CTL and NT runs must play a more determinant role in the subsequent evolution and intensification of the vortex after vortex shedding. It is known that both a stronger initial vortex and favorable synoptic evolution surrounding it are important to TC genesis (section 1), in addition to mesoscale convection and nonlinear interactions. In section 3, low-level northeasterly winds across or near northern Sumatra, equatorial WWBs at low latitudes, and advection of vorticity and/or moisture from upstream into the lee area are seen to be the common ingredients in all four cases of 03A, Nisha, 07B, and Ward (Figs. 3–5). To find out how frequently these conditions/features occur for the TCs, here we use the ECMWF-YOTC data to check their occurrence in all 22 vortices in the tropical NIO that appeared west of 90°E and possessed closed circulation for at least 24 h at 925 hPa during October–December in 2008 and 2009 (including those not tied to Sumatra) following the same procedure as in section 3. The overall results are presented in Fig. 20.

In Fig. 20, the time series of equatorial westerly wind speed (averaged also over 5°S–5°N, 80°–90°E) and northeasterly wind speed (averaged over 5°–10°N, 107°–115°E), both at 925 hPa, are shown together with the periods with storms tracked by JTWC and those with vorticity (pink) and/or water vapor advection (orange) at 700 hPa (above Sumatra's terrain). While the low-level northeasterly winds generally strengthen from October to December and the equatorial westerly winds tend to be stronger in November, both of them are characterized by surges or pulses. During their early stage, the majority of vortices were associated with simultaneous surges in both northeasterly flow near northern Sumatra and equatorial westerly flow (Fig. 20). Among the seven cases that reached TS, the only exception is Phyan (2009), where the equatorial westerly was weak and only 2–3 m s^{-1} (Fig. 20b). During the formation stage, many disturbances were also accompanied by either vorticity or moisture advection, or both, especially in the Bay of Bengal (BOB) where many vortices originated from the lee side of Sumatra. Thus, not only in the four cases in section 3 (Figs. 2–5), the low-level environment that provided a background of cyclonic wind shear and the advection of vorticity/moisture from upstream into the area of initial vortex were also common features in nearly all cases in October–December of 2008 and 2009. Thus, these synoptic features are

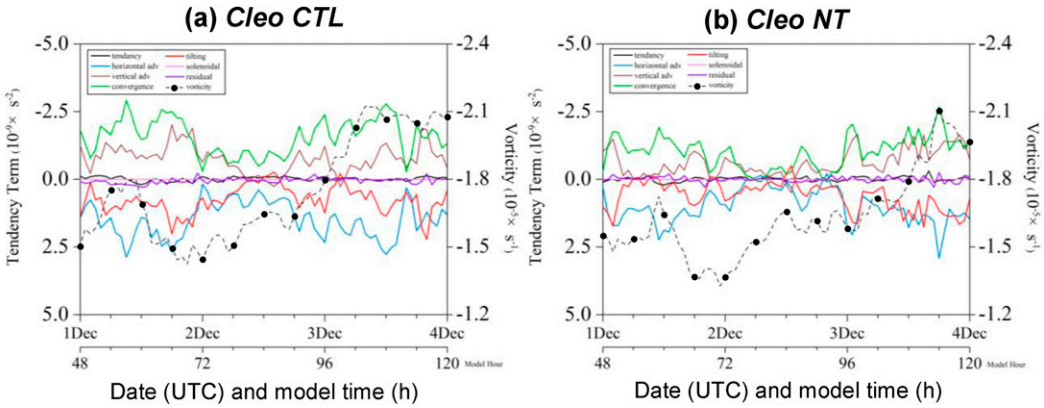

FIG. 18. As in Fig. 9, but for Cleo from 0000 UTC 1 Dec to 0000 UTC 4 Dec 2009. Note that the vertical scale is reversed for this case in the Southern Hemisphere.

undoubtedly important factors for the development of initial vortices toward the TS/TC status in the NIO. Due to these favorable factors (and a positive interaction with the convection) in the cases of Nisha and Ward, a similar vortex can still develop to reach TS status even in the NT runs when Sumatra's topography is removed in the model. In eastern Pacific, an analogous situation exists, as many easterly wave disturbances there can be traced back to those from the North Atlantic crossing Central America (Rydbeck et al. 2017).

Based on the findings in this study, a modified conceptual model from Kuettner (1967, 1989; Fig. 1a) is presented below in Fig. 21. In the NIO, the northeasterly wind (from upstream across the Malaysia Peninsula) near the northern tip of Sumatra combines with the equatorial westerly wind surge to provide a favorable background shear for the lee vortex to evolve. Frequently, the lee vortices are maintained and enhanced by incipient disturbances (a BV or TC/TS remnant) from the SCS, in the form of vorticity and/or moisture advection into the lee side. In these cases, the topography of Sumatra can provide additional help through flow deflection and lee cyclogenesis to further enhance the vorticity during the lee stage, but it is not a necessary factor. For SIO, Cleo (2009) is the only storm studied herein. In this case, the northeasterly wind did not reach the southern latitudes, and southwestern Sumatra is on the windward side instead of lee side due to the equatorial westerly wind. However, Sumatra played a role to deflect the westerly wind southward and provide a larger vorticity together with the southeasterly trade wind farther south. Thus, the hypothesis of Fine et al. (2016) is confirmed and the topography is also helpful for TC formation, and the synoptic conditions remain favorable for dual-vortex formation across the equator (as in the case of Ward and Cleo). In contrast to the original model proposed by Kuettner (1967, 1989) in Fig. 1a, our conceptual model (Fig. 21) also includes the roles of equatorial westerly wind and upstream incipient disturbances from the SCS, with a different formation scenario for the vortex in SIO, namely, not at the lee side of topography.

7. Summary and conclusions

Building upon the observational study of Fine et al. (2016), the present work has selected a few of their cases for more detailed analysis and three cases for high-resolution numerical simulation and sensitivity test to investigate the role played by the island of Sumatra in subsequent TC formation in the IO. The CReSS model employed has a convective-permitting 4-km grid size and large domain of $5600 \times 4464\,\mathrm{km}^2$ (Table 1), and the

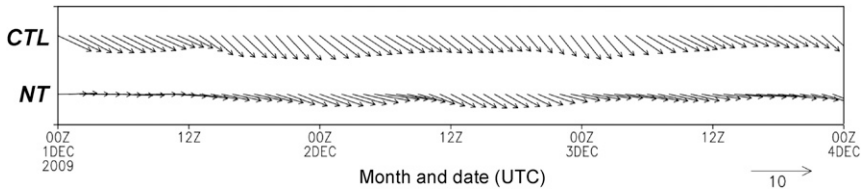

FIG. 19. Averaged low-level horizontal wind (m s^{-1}, over 50–1913 m) in the northeastern quadrant of Cleo at 1-h intervals from 0000 UTC 1 Dec to 0000 UTC 4 Dec 2009 in CTL and NT experiments.

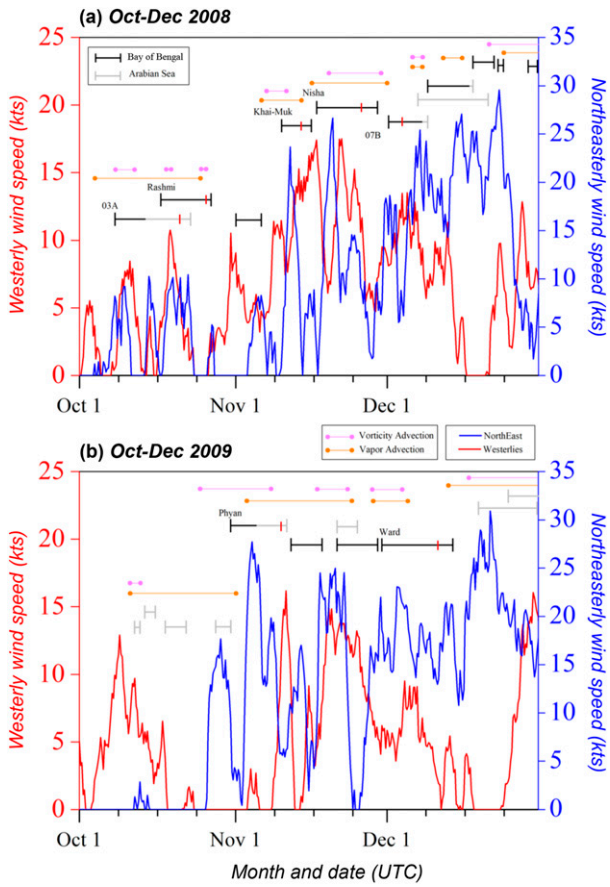

FIG. 20. Time series of westerly wind speed in equatorial IO (kt, red, averaged over 5°S–5°N, 80°–90°E) and northeasterly wind speed east of northern Sumatra (kt, blue, averaged over 5°–10°N, 107°–115°E) at 925 hPa in the ECMWF-YOTC data during October–December of (a) 2008 and (b) 2009. Black/gray segments indicate periods with a closed vortex in BOB/Arabian Sea (divided at 80°E) with named storms labeled (the naming times shown by short red ticks). The periods with 700-hPa positive vorticity advection (pink) and moisture advection (orange) at the SCS are also marked.

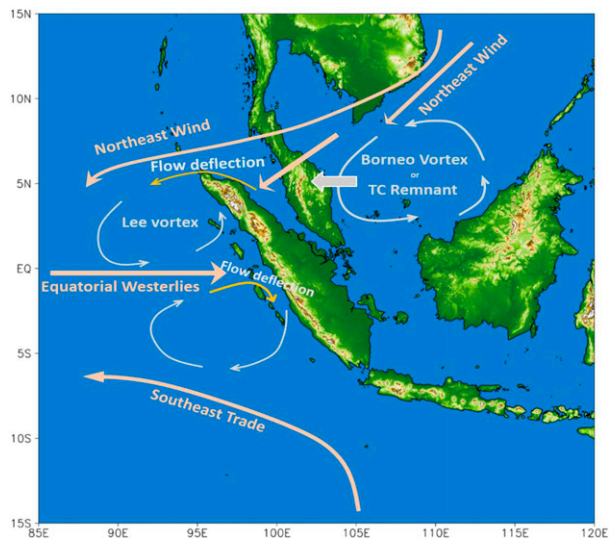

FIG. 21. Schematics for synoptic conditions favorable for the formation of lee vortices to the west of Sumatra that may subsequently develop into TCs in the IO during the postmonsoon period (October–December), obtained in this study. These factors include vorticity and moisture advection from the SCS (linked to TC remnant or BV), prevailing northeasterly (southeasterly) winds in NH (SH), and the deflection of low-level northeasterly wind by the northern part (westerly wind by the southern part) of Sumatra for the northern (southern) vortex.

simulations for the three cases, including Nisha (2008) in NIO and the TC pairs of Ward and Cleo (2009), are for at least 15 days. In the CTL runs, the evolution of the vortices, including the lee stage (for Nisha and Ward), is reasonably well captured. The results are then compared and contrasted to those in the sensitivity tests (NT runs), in which the topography of Sumatra is removed. The major findings of the present study can be summarized below.

1) In the NT tests without Sumatra topography, the three TC cases initiate in approximately the same location and also all reach TS status as in the CTL experiment and observation, but tend to do so at a later time. This time difference is 27 h for Nisha (2008), 12 h for Cleo (2009), and only 4 h for Ward (2009). The island of Sumatra therefore is not a necessary condition for TC genesis in the IO, as expected.
2) During the leeside stage of Nisha and Ward in NIO, both vortices in the CTL runs tend to possess a slightly stronger areal-mean vorticity in the low level compared to their counterpart in NT runs. A vorticity budget analysis indicates that the main contributing terms are vertical stretching and vertical advection at the lee side. Thus, the Sumatra topography appears helpful in producing a larger vorticity and stronger initial vortex for subsequent development after vortex shedding.
3) For the four NIO cases examined, easterly or northeasterly winds near the northern tip of Sumatra, equatorial westerly wind surge, and advection of vorticity and moisture from upstream (either a TC/TS remnant or a BV) are common synoptic features at (or near) the formation of the lee vortex. A more extensive examination of 22 vortices in October–December of 2008 and 2009 suggests that these favorable factors were also frequently present, especially in those that reached TS status in the BOB. Evidently, with these features and their associated environment, the convection and nonlinear interactions lead to the intensification of the vortex in NT runs, often from a (slightly) weaker vortex without Sumatra topography.

4) For Cleo (2009) in SIO, the formation area is not at lee but windward side due to the presence of equatorial westerly wind surge, as analyzed by Fine et al. (2016). The Sumatra topography in this case has a deflection effect on the westerly, and thereby provides stronger vorticity (in combination with southeasterly wind farther south). Subsequently, the inner vortex in CTL remains stronger and reaches TS status earlier than its counterpart in the NT experiment.
5) A conceptual model is presented in Fig. 21, which summarizes the above results and depicts the favorable conditions for TC genesis in NIO from initial vortex from the lee side of Sumatra as well as SIO. For NIO, these include northeasterly wind near 5°–10°N, equatorial WWB, and advection of vorticity/moisture from SCS. For SIO cases, they include the southward flow deflection of westerlies and southeasterly trade wind at higher latitudes.

The simulation results of Nisha (2008) and Ward (2009) and the conceptual model obtained here are likely applicable to many TCs in the NIO that originate from the lee of Sumatra, but presumably not all of them. More high-resolution simulations are recommended in the future to further explore the potential role played by the Sumatra topography on TC formation, including those in the SIO. An ensemble approach is also recommended to adequately address the uncertainty issue in deterministic simulations of chaotic systems (i.e., to properly isolate the differences caused by the topography from those arising from nonlinearity).

Acknowledgments. The authors wish to thank the four anonymous reviewers, as well as Prof. C.-S. Lee of the National Taiwan University, for their helpful comments that lead to significant improvement of the manuscript. The ECMWF and YOTC project is acknowledged for making available the gridded analysis data. The TRMM PR/TMI observations in Figs. 7, 12, and 16 are provided by the NRL, and Ms. Shin-Yi Huang also helped with the plotting. This study is jointly supported by the Ministry of Science and Technology (MOST) of Taiwan under Grants MOST-105-2111-M-003-003-MY3, MOST-108-2111-M-003-005-MY2, and MOST-108-2625-M-003-001. Richard Johnson acknowledges support under National Science Foundation (NSF) under Grants AGS-1360237 and AGS-1853633.

REFERENCES

Chang, C.-P., C.-H. Liu, and H.-C. Kuo, 2003: Typhoon Vamei: An equatorial tropical cyclone formation. *Geophys. Res. Lett.*, **30**, 1150, https://doi.org/10.1029/2002GL016365.

——, P. A. Harr, and H. J. Chen, 2005: Synoptic disturbances over the equatorial South China Sea and western Maritime Continent during boreal winter. *Mon. Wea. Rev.*, **133**, 489–503, https://doi.org/10.1175/MWR-2868.1.

Charney, J. G., and A. Eliassen, 1964: On the growth of the hurricane depression. *J. Atmos. Sci.*, **21**, 68–75, https://doi.org/10.1175/1520-0469(1964)021<0068:OTGOTH>2.0.CO;2.

Chen, Y.-H., H.-C. Kuo, C.-C. Wang, and Y.-T. Yang, 2017: Influence of southwest monsoon flow and typhoon track on Taiwan rainfall during the exit phase: Modeling study of Typhoon Morakot (2009). *Quart. J. Roy. Meteor. Soc.*, **143**, 3014–3024, https://doi.org/10.1002/qj.3156.

Cotton, W. R., G. J. Tripoli, R. M. Rauber, and E. A. Mulvihill, 1986: Numerical simulation of the effects of varying ice crystal nucleation rates and aggregation processes on orographic snowfall. *J. Climate Appl. Meteor.*, **25**, 1658–1680, https://doi.org/10.1175/1520-0450(1986)025<1658:NSOTEO>2.0.CO;2.

Deardorff, J. W., 1980: Stratocumulus-capped mixed layers derived from a three-dimensional model. *Bound.-Layer Meteor.*, **18**, 495–527, https://doi.org/10.1007/BF00119502.

Emanuel, K. A., 1986: An air-sea interaction theory for tropical cyclones. Part I: Steady-state maintenance. *J. Atmos. Sci.*, **43**, 585–605, https://doi.org/10.1175/1520-0469(1986)043<0585:AASITF>2.0.CO;2.

Epifanio, C. C., 2003: Lee vortices. *Encyclopedia of Atmospheric Sciences*, J. R. Holton, J. Pyle, and J. A. Curry, Eds., Elsevier Science Ltd., 1150–1160.

——, and D. R. Durran, 2001: Three-dimensional effects in high-drag-state flows over long ridges. *J. Atmos. Sci.*, **58**, 1051–1065, https://doi.org/10.1175/1520-0469(2001)058<1051:TDEIHD>2.0.CO;2.

Farfán, L. M., and J. A. Zehnder, 1997: Orographic influence on the synoptic-scale circulations associated with the genesis of Hurricane Guillermo (1991). *Mon. Wea. Rev.*, **125**, 2683–2698, https://doi.org/10.1175/1520-0493(1997)125<2683:OIOTSS>2.0.CO;2.

Fine, C. M., R. H. Johnson, P. E. Ciesielski, and R. K. Taft, 2016: The role of topographically induced vortices in tropical cyclone formation over the Indian Ocean. *Mon. Wea. Rev.*, **144**, 4827–4847, https://doi.org/10.1175/MWR-D-16-0102.1.

Gray, W. M., 1968: Global view of the origins of tropical disturbances and storms. *Mon. Wea. Rev.*, **96**, 669–700, https://doi.org/10.1175/1520-0493(1968)096<0669:GVOTOO>2.0.CO;2.

Ikawa, M., and K. Saito, 1991: Description of a nonhydrostatic model developed at the Forecast Research Department of the MRI. MRI Tech. Rep. 28, 238 pp.

Johnson, R. H., and P. E. Ciesielski, 2013: Structure and properties of Madden–Julian Oscillations deduced from DYNAMO sounding arrays. *J. Atmos. Sci.*, **70**, 3157–3179, https://doi.org/10.1175/JAS-D-13-065.1.

Kikuchi, K., and B. Wang, 2010: Formation of tropical cyclones in the northern Indian Ocean associated with two types of tropical intraseasonal oscillation modes. *J. Meteor. Soc. Japan*, **88**, 475–496, https://doi.org/10.2151/jmsj.2010-313.

Kondo, J., 1976: Heat balance of the China Sea during the air mass transformation experiment. *J. Meteor. Soc. Japan*, **54**, 382–398, https://doi.org/10.2151/jmsj1965.54.6_382.

Kuettner, J. P., 1967: The equatorial double vortex: Unique hydrodynamic role of Sumatra in atmospheric developments over the Indian Ocean. *Bull. Amer. Meteor. Soc.*, **48**, 637.

——, 1989: Easterly flow over the cross equatorial island of Sumatra and its role in the formation of cyclone pairs over the Indian Ocean. *Wetter Leben*, **41**, 47–55.

Kuo, H.-C., S. Tsujino, C.-C. Huang, C.-C. Wang, and K. Tsuboki, 2019: Diagnosis of the dynamic efficiency of latent heat release

and the rapid intensification of Supertyphoon Haiyan (2013). *Mon. Wea. Rev.*, **147**, 1127–1147, https://doi.org/10.1175/MWR-D-18-0149.1.

Lee, C.-S., 1986: An observational study of tropical cloud cluster evolution and cyclogenesis in the western North Pacific. Department of Atmospheric Science Paper 403, Colorado State University, 250 pp.

——, R. Edson, and W. M. Gray, 1989: Some large-scale characteristics associated with tropical cyclone development in the North Indian Ocean during FGGE. *Mon. Wea. Rev.*, **117**, 407–426, https://doi.org/10.1175/1520-0493(1989)117<0407:SLSCAW>2.0.CO;2.

Lin, Y.-L., and C.-S. Lee, 2011: An analysis of tropical cyclone formations in the South China Sea during the late season. *Mon. Wea. Rev.*, **139**, 2748–2760, https://doi.org/10.1175/2011MWR3495.1.

——, R. D. Farley, and H. D. Orville, 1983: Bulk parameterization of the snow field in a cloud model. *J. Climate Appl. Meteor.*, **22**, 1065–1092, https://doi.org/10.1175/1520-0450(1983)022<1065:BPOTSF>2.0.CO;2.

Louis, J. F., M. Tiedtke, and J. F. Geleyn, 1982: A short history of the operational PBL parameterization at ECMWF. *Workshop on Planetary Boundary Layer Parameterization*, Reading, United Kingdom, ECMWF, 59–79.

Love, G., 1985a: Cross-equatorial influence of winter hemisphere subtropical cold surges. *Mon. Wea. Rev.*, **113**, 1487–1498, https://doi.org/10.1175/1520-0493(1985)113<1487:CEIOWH>2.0.CO;2.

——, 1985b: Cross-equatorial interaction during tropical cyclone genesis. *Mon. Wea. Rev.*, **113**, 1499–1509, https://doi.org/10.1175/1520-0493(1985)113<1499:CEIDTC>2.0.CO;2.

Moncrieff, M. W., D. E. Waliser, M. J. Miller, M. A. Shapiro, G. R. Asrar, and J. Caughey, 2012: Multiscale convective organization and the YOTC virtual global field campaign. *Bull. Amer. Meteor. Soc.*, **93**, 1171–1187, https://doi.org/10.1175/BAMS-D-11-00233.1.

Mozer, J. B., and J. A. Zehnder, 1996: Lee vorticity production by large-scale tropical mountain ranges. Part I: Eastern North Pacific tropical cyclogenesis. *J. Atmos. Sci.*, **53**, 521–538, https://doi.org/10.1175/1520-0469(1996)053<0521:LVPBLS>2.0.CO;2.

Murakami, M., 1990: Numerical modeling of dynamical and microphysical evolution of an isolated convective cloud—The 19 July 1981 CCOPE cloud. *J. Meteor. Soc. Japan*, **68**, 107–128, https://doi.org/10.2151/jmsj1965.68.2_107.

——, T. L. Clark, and W. D. Hall, 1994: Numerical simulations of convective snow clouds over the Sea of Japan: Two-dimensional simulation of mixed layer development and convective snow cloud formation. *J. Meteor. Soc. Japan*, **72**, 43–62, https://doi.org/10.2151/jmsj1965.72.1_43.

Ooyama, K. V., 1982: Conceptual evolution of the theory and modeling of the tropical cyclone. *J. Meteor. Soc. Japan*, **60**, 369–380, https://doi.org/10.2151/jmsj1965.60.1_369.

Ritchie, E. A., and G. J. Holland, 1999: Large-scale patterns associated with tropical cyclogenesis in the western Pacific. *Mon. Wea. Rev.*, **127**, 2027–2043, https://doi.org/10.1175/1520-0493(1999)127<2027:LSPAWT>2.0.CO;2.

Rotunno, R., and K. A. Emanuel, 1987: An air-sea interaction theory for tropical cyclones. Part II: Evolutionary study using a nonhydrostatic axisymmetric numerical model. *J. Atmos. Sci.*, **44**, 542–561, https://doi.org/10.1175/1520-0469(1987)044<0542:AAITFT>2.0.CO;2.

——, and P. K. Smolarkiewicz, 1991: Further results on lee vortices in low-Froude-number flow. *J. Atmos. Sci.*, **48**, 2204–2211, https://doi.org/10.1175/1520-0469(1991)048<2204:FROLVI>2.0.CO;2.

Rydbeck, A. V., E. C. Maloney, and G. J. Alaka Jr., 2017: In situ initiation of East Pacific easterly waves in a regional model. *J. Atmos. Sci.*, **74**, 333–351, https://doi.org/10.1175/JAS-D-16-0124.1.

Segami, A., K. Kurihara, H. Nakamura, M. Ueno, I. Takano, and Y. Tatsumi, 1989: Operational mesoscale weather prediction with Japan Spectral Model. *J. Meteor. Soc. Japan*, **67**, 907–924, https://doi.org/10.2151/JMSJ1965.67.5_907.

Smolarkiewicz, P. K., and R. Rotunno, 1989: Low Froude number flow past three-dimensional obstacles. Part I: Baroclinically generated lee vortices. *J. Atmos. Sci.*, **46**, 1154–1164, https://doi.org/10.1175/1520-0469(1989)046<1154:LFNFPT>2.0.CO;2.

Subbaramayya, I., and S. R. M. Rao, 1984: Frequency of Bay of Bengal cyclones in the post-monsoon season. *Mon. Wea. Rev.*, **112**, 1640–1642, https://doi.org/10.1175/1520-0493(1984)112<1640:FOBOBC>2.0.CO;2.

Takahashi, H. G., Y. Fukutomi, and J. Matsumoto, 2011: The impact of long-lasting northerly surges of the East Asian winter monsoon on tropical cyclogenesis and its seasonal march. *J. Meteor. Soc. Japan*, **89A**, 181–200, https://doi.org/10.2151/jmsj.2011-A12.

Tsuboki, K., and A. Sakakibara, 2002: Large-scale parallel computing of cloud resolving storm simulator. *High Performance Computing*, H. P. Zima et al., Eds., Springer, 243–259.

——, and ——, 2007: *Numerical Prediction of High-Impact Weather Systems: The Textbook for the Seventeenth IHP Training Course in 2007*. Hydrospheric Atmospheric Research Center, Nagoya University, and UNESCO, 273 pp.

Waliser, D. E., and Coauthors, 2012: The "year" of tropical convection (May 2008–April 2010): Climate variability and weather highlights. *Bull. Amer. Meteor. Soc.*, **93**, 1189–1218, https://doi.org/10.1175/2011BAMS3095.1.

Wang, C.-C., 2015: The more rain, the better the model performs—The dependency of quantitative precipitation forecast skill on rainfall amount for typhoons in Taiwan. *Mon. Wea. Rev.*, **143**, 1723–1748, https://doi.org/10.1175/MWR-D-14-00137.1.

——, H.-C. Kuo, Y.-H. Chen, H.-L. Huang, C.-H. Chung, and K. Tsuboki, 2012: Effects of asymmetric latent heating on typhoon movement crossing Taiwan: The case of Morakot (2009) with extreme rainfall. *J. Atmos. Sci.*, **69**, 3172–3196, https://doi.org/10.1175/JAS-D-11-0346.1.

——, Y.-H. Chen, H.-C. Kuo, and S.-Y. Huang, 2013: Sensitivity of typhoon track to asymmetric latent heating/rainfall induced by Taiwan topography: A numerical study of Typhoon Fanapi (2010). *J. Geophys. Res. Atmos.*, **118**, 3292–3308, https://doi.org/10.1002/JGRD.50351.

——, H.-C. Kuo, R. H. Johnson, C.-Y. Lee, S.-Y. Huang, and Y.-H. Chen, 2015: A numerical study of convection in rainbands of Typhoon Morakot (2009) with extreme rainfall: Roles of pressure perturbations with low-level wind maxima. *Atmos. Chem. Phys.*, **15**, 11 097–11 115, https://doi.org/10.5194/acp-15-11097-2015.

——, S.-Y. Huang, S.-H. Chen, C.-S. Chang, and K. Tsuboki, 2016: Cloud-resolving typhoon rainfall ensemble forecasts for Taiwan with large domain and extended range through time-lagged approach. *Wea. Forecasting*, **31**, 151–172, https://doi.org/10.1175/WAF-D-15-0045.1.

Zehnder, J. A., D. M. Powell, and D. L. Ropp, 1999: The interaction of easterly waves, orography, and the intertropical convergence zone in the genesis of eastern Pacific tropical cyclones. *Mon. Wea. Rev.*, **127**, 1566–1585, https://doi.org/10.1175/1520-0493(1999)127<1566:TIOEWO>2.0.CO;2.